

International Journal of Modern Physics A
 © World Scientific Publishing Company

Charm Meson Mixing: An Experimental Review

Carlos A. Chavez

PH Department, CERN

1211 Geneva 23

Switzerland

carlos.chavez.barajas@cern.ch

Ray F. Cowan

Lepton Quark Studies Group, Laboratory for Nuclear Science, M.I.T., 77 Massachusetts Avenue

Cambridge, Massachusetts 02139, USA

rcowan@mit.edu

W.S. Lockman

University of California at Santa Cruz, Institute for Particle Physics

Santa Cruz, California 95064, USA

lockman@slac.stanford.edu

Received Day Month Year

Revised Day Month Year

We review current experimental results on charm mixing and CP violation. We survey experimental techniques, including time-dependent, time-independent, and quantum-correlated measurements. We review techniques that use a slow pion tag from $D^{*+} \rightarrow \pi^+ D^0 + \text{c.c.}$ decays and those that do not, and cover two-body and multi-body D^0 decay modes. We provide a summary of D -mixing results to date and comment on future experimental prospects at the LHC and other new or planned facilities.

Keywords: Charm; mixing; CP violation.

PACS numbers: 13.25Ft, 11.30Er, 12.15Ff, 14.40Lb

1. Introduction

Quantum-mechanical mixing between neutral meson particle and anti-particle flavor eigenstates provides important information about electroweak interactions and the Cabibbo-Kobayashi-Maskawa (CKM) matrix, as well as the virtual particles that are exchanged in the mixing process itself. The two parameters characterizing D^0 - \bar{D}^0 mixing are

$$x \equiv \frac{\Delta M}{\Gamma}, \quad \Delta M \equiv M_1 - M_2 \quad (1)$$

$$y \equiv \frac{\Delta \Gamma}{2\Gamma}, \quad \Delta \Gamma \equiv \Gamma_1 - \Gamma_2 \quad (2)$$

where $M_{1,2}$ are the masses of $D_{1,2}$, $\Gamma_{1,2}$ are the decay widths, and $\Gamma \equiv (\Gamma_1 + \Gamma_2)/2$ is the mean decay width.

Mixing between the states K^0 and \bar{K}^0 , B^0 and \bar{B}^0 , and B_s and \bar{B}_s is well established. Mixing in these systems is well described by standard model (SM) box diagrams containing up-type (u, c, t) quarks. In contrast, the $D^0\text{-}\bar{D}^0$ SM mixing amplitude at short distances involves loops containing down-type (d, s, b) quarks. The s and d box amplitudes¹ together are suppressed by a factor $(m_s^2 - m_d^2)^2 / (m_W^2 m_c^2)$ due to the Glashow-Iliopoulos-Maiani (GIM) mechanism, while the contribution from loops involving b quarks is further suppressed by the Cabibbo-Kobayashi-Maskawa (CKM) factor $|V_{ub}V_{cb}^*|^2 / |V_{us}V_{cs}^*|^2 = \mathcal{O}(10^{-6})$. The contribution of the box diagrams shown in Fig. 1(a–b) to x is $x^{box} \approx 5 \times 10^{-6} [m_s/0.2 \text{ GeV}/c^2]^4$.² The di-penguin diagram shown in Fig. 1(c) contributes at a similar level, but with opposite sign.² Such diagrams contribute only to x . A perturbative QCD next-to-leading order (NLO) analysis of $D^0\text{-}\bar{D}^0$ mixing³ using an operator product expansion^{4,5,6} to evaluate $\Delta\Gamma$ in terms of local $|\Delta C| = 1$ operators, followed by a dispersion relation to evaluate ΔM ,⁷ obtains: $x, y \simeq 6 \times 10^{-7}$. Taken together, the short-distance SM predictions are $x \sim \mathcal{O}(10^{-5})$, $y \sim \mathcal{O}(10^{-7})$, far below the current measurements, $x, y \sim \mathcal{O}(10^{-2})$.

The long-distance contributions to $D^0\text{-}\bar{D}^0$ mixing are inherently nonperturbative and thus difficult to estimate. There are two approaches to estimating $D^0\text{-}\bar{D}^0$ mixing in the SM: An inclusive approach uses the Operator Product Expansion and quark-hadron duality to expand x and y in terms of local operators.^{4,5,6} If the charm quark mass m_c is large compared to the scale of strong interactions, the series can be truncated after a few terms. Such calculations typically yield $x, y \leq 10^{-3}$. The exclusive approach sums over intermediate hadronic states to which both D^0 and \bar{D}^0 can decay, as shown schematically in Fig. 2. Here, non-vanishing y arises from $SU(3)_F$ breaking in decay rates when summing over intermediate states within an $SU(3)_F$ multiplet. Ref. 8 found that $SU(3)_F$ violation in the final state phase space could provide enough $SU(3)_F$ breaking to generate $y \sim 10^{-2}$. Ref. 7 used a dispersion relation to relate x to y and found x to be in the range $(-1.0, -0.1) \times y$.

New physics (NP) processes, some examples of which are shown in Figs. 1(d–f), could enhance the $D^0\text{-}\bar{D}^0$ mixing rate to the level of experimental detection, but the predictions for these rates also span many orders of magnitude.^{9,10,11} Given the uncertainties in both the SM and NP calculations, observation of $D^0\text{-}\bar{D}^0$ mixing at $\mathcal{O}(10^{-2})$ does not unambiguously indicate the presence of new physics. See Refs. 9 and 10 for a summary of $D^0\text{-}\bar{D}^0$ mixing parameter predictions.

Evidence for $D^0\text{-}\bar{D}^0$ mixing was reported in 2007 using high-luminosity data sets acquired at the B factories^{12,13} and Tevatron collider.¹⁴ While the significance of the current world average for $D^0\text{-}\bar{D}^0$ mixing is greater than ten standard deviations (10σ),¹⁵ to date no one single $D^0\text{-}\bar{D}^0$ mixing measurement exceeds 5σ , the commonly accepted criterion for observation.

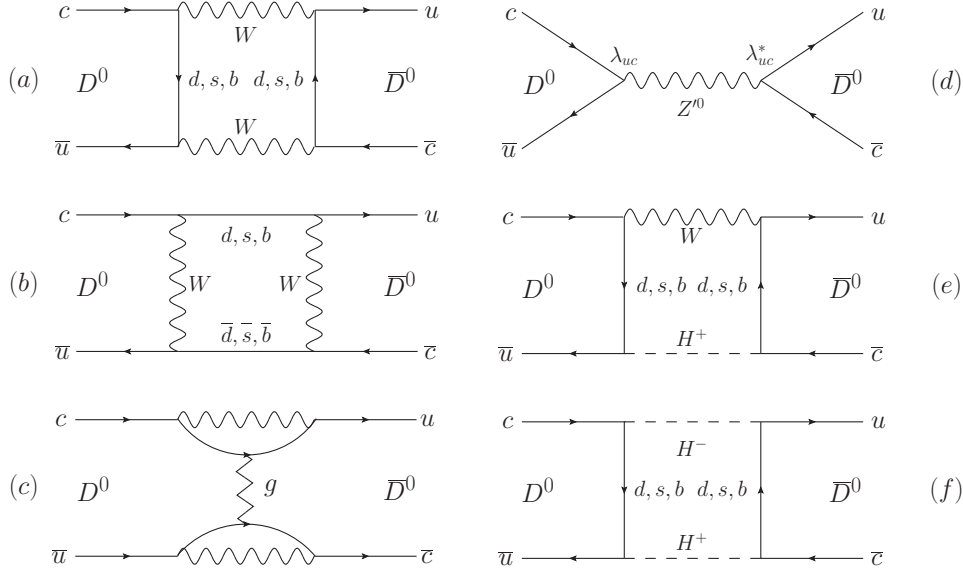


Fig. 1. Possible short-distance amplitudes contributing to D^0 - \bar{D}^0 mixing. (a–b) SM boxes; (c) SM di-penguin; (d): new physics flavor-changing neutral current process mediated by a heavy Z'^0 ; (e–f): charged Higgs in the mixing loop.

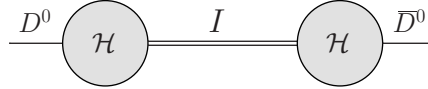


Fig. 2. Long-distance contribution from an intermediate state I to D^0 - \bar{D}^0 mixing. \mathcal{H} is the Hamiltonian governing weak decays. From Ref. 16.

1.1. D^0 - \bar{D}^0 Mixing Formalism

The D^0 and \bar{D}^0 mesons are produced as flavor eigenstate with charm quantum numbers $C = +1$ and -1 , respectively. They propagate and decay according to the Schrödinger equation:

$$i \frac{\partial}{\partial t} \begin{pmatrix} D^0(t) \\ \bar{D}^0(t) \end{pmatrix} = \left(\mathbf{M} - \frac{i}{2} \mathbf{\Gamma} \right) \begin{pmatrix} D^0(t) \\ \bar{D}^0(t) \end{pmatrix}. \quad (3)$$

Mixing between D^0 and \bar{D}^0 occurs because these flavor states are not the eigenstates D_1 and D_2 of the D^0 - \bar{D}^0 mass matrix $\mathbf{M} - i\mathbf{\Gamma}/2$, but linear combinations of them. Assuming that the product of charge conjugation, parity and time reversal (CPT) is conserved,¹⁷ the eigenstates of Eq. 3, $|D_{1,2}\rangle$ are given by:^{17,18}

$$\begin{aligned} |D_1\rangle &= p|D^0\rangle + q|\bar{D}^0\rangle, \\ |D_2\rangle &= p|D^0\rangle - q|\bar{D}^0\rangle, \end{aligned} \quad (4)$$

4 Chavez, Cowan, and Lockman

and inversely

$$\begin{aligned} |D^0\rangle &= \frac{1}{2p} (|D_1\rangle + |D_2\rangle), \\ |\bar{D}^0\rangle &= \frac{1}{2q} (|D_1\rangle - |D_2\rangle), \end{aligned} \quad (5)$$

where the complex quantities p and q satisfy

$$\left(\frac{q}{p}\right)^2 = \frac{M_{12}^* - \frac{i}{2}\Gamma_{12}^*}{M_{12} - \frac{i}{2}\Gamma_{12}}, \quad |p|^2 + |q|^2 = 1, \quad (6)$$

where M_{12} and Γ_{12} are the complex off-diagonal elements of the 2×2 matrices \mathbf{M} and $\mathbf{\Gamma}$, respectively. In the limit of CP conservation, D_1 is CP -even and D_2 is CP -odd.^a The eigenvalues of Eq. 3 are:

$$\gamma_{1,2} \equiv M_{1,2} - \frac{i}{2}\Gamma_{1,2} = M_{11} - \frac{i}{2}\Gamma_{11} \pm \frac{q}{p} \left(M_{12} - \frac{i}{2}\Gamma_{12} \right) \quad (7)$$

The eigenstates of Eq. 3 develop in time as follows:^{17,18}

$$|D_{1,2}(t)\rangle = e_{1,2}(t)|D_{1,2}(0)\rangle, \quad e_{1,2}(t) \equiv \exp \left[-i \left(M_{1,2} - \frac{i}{2}\Gamma_{1,2} \right) t \right], \quad (8)$$

Using Eq. 4, Eq. 5 and Eq. 8, the proper time evolution of a state which is initially a pure D^0 (\bar{D}^0) is given by:

$$|D^0(t)\rangle = g_+(t)|D^0\rangle + \frac{q}{p}g_-(t)|\bar{D}^0\rangle, \quad (9)$$

$$|\bar{D}^0(t)\rangle = g_+(t)|\bar{D}^0\rangle + \frac{p}{q}g_-(t)|D^0\rangle. \quad (10)$$

where:

$$g_{\pm}(t) = [e_1(t) \pm e_2(t)] / 2. \quad (11)$$

The probabilities for obtaining a D^0 or \bar{D}^0 at proper time t , starting from an initially pure D^0 or \bar{D}^0 are:

$$\begin{aligned} |\langle D^0 | D^0(t) \rangle|^2 &= |\langle \bar{D}^0 | \bar{D}^0(t) \rangle|^2 \\ &= |g_+(t)|^2 = \frac{1}{2} e^{-\Gamma t} [\cosh(y\Gamma t) + \cos(x\Gamma t)], \end{aligned} \quad (12)$$

$$|\langle \bar{D}^0 | D^0(t) \rangle|^2 = \left| \frac{q}{p} \right|^2 |g_-(t)|^2 = \frac{1}{2} \left| \frac{q}{p} \right|^2 e^{-\Gamma t} [\cosh(y\Gamma t) - \cos(x\Gamma t)], \quad (13)$$

$$|\langle D^0 | \bar{D}^0(t) \rangle|^2 = \left| \frac{p}{q} \right|^2 |g_-(t)|^2 = \frac{1}{2} \left| \frac{p}{q} \right|^2 e^{-\Gamma t} [\cosh(y\Gamma t) - \cos(x\Gamma t)], \quad (14)$$

If both x and y are zero, then the probability for a D^0 to mix to a \bar{D}^0 or for a \bar{D}^0 to mix to a D^0 will be identically zero for all proper times. If either x or y is non-zero, then D^0 - \bar{D}^0 mixing will occur.

^aWe use the CP phase convention: $CP|D^0\rangle = +|\bar{D}^0\rangle$ and $CP|\bar{D}^0\rangle = +|D^0\rangle$.

M_{12} and Γ_{12} determine the mass and width splittings ΔM and $\Delta\Gamma$, respectively:

$$\Delta M \equiv M_1 - M_2 = 2\text{Re} \left[\frac{q}{p} (M_{12} - \frac{i}{2}\Gamma_{12}) \right] \quad (15)$$

$$\Delta\Gamma \equiv \Gamma_1 - \Gamma_2 = -4\text{Im} \left[\frac{q}{p} (M_{12} - \frac{i}{2}\Gamma_{12}) \right], \quad (16)$$

and therefore the characteristics of $D^0\bar{D}^0$ mixing. We show the unmixed and mixed intensities as a function of the dimensionless variable, Γt , for initially pure states of K^0 , D^0 , B^0 and B_s , in Figs. 3(a-d), respectively. Of the four lowest-lying neutral pseudoscalar meson systems, the $D^0\bar{D}^0$ system shows the smallest mixing, as noted earlier. In the K^0 system, both $|x|$ and $|y|$ are both of order 1; in the D^0 system, $|x|$ and $|y|$ are both of order 1%; in the B^0 and B_s systems, $|x| \gg |y|$.

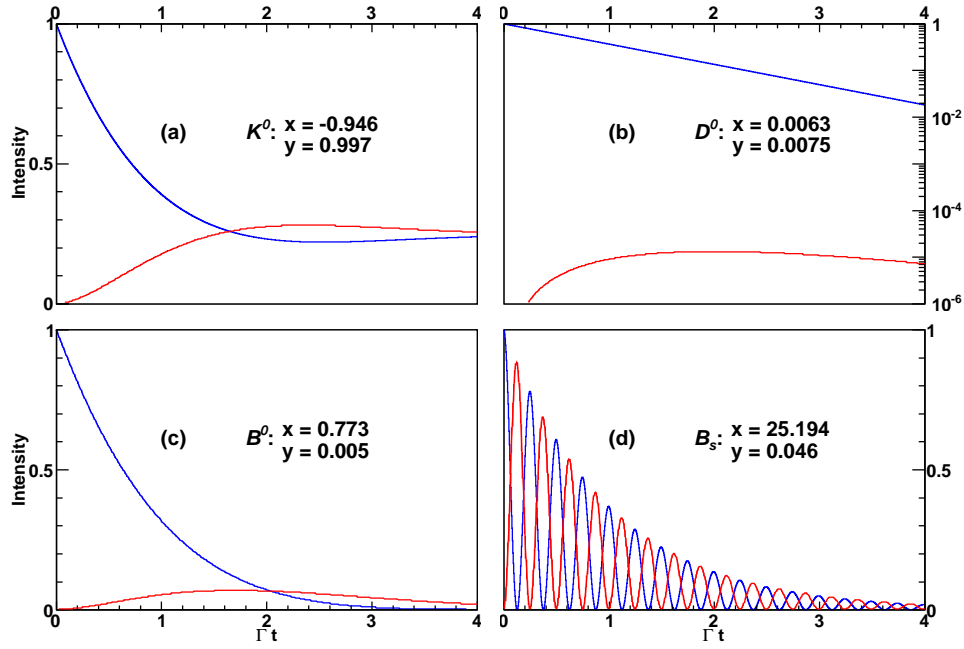


Fig. 3. The unmixed (blue) and mixed (red) intensities for an initially pure (a) K^0 ; (b) D^0 ; (c) B^0 ; (d) B_s state. The vertical scale in (b) is logarithmic, the others linear. The values of the mixing parameters as defined in Eqs. 1 and 2 are obtained using data from Ref. 19, assuming $||q/p| = 1$.

From Eq. 9 (Eq. 10), the amplitude that a D^0 (\bar{D}^0) produced at $t = 0$ will develop into a linear combination of D^0 and \bar{D}^0 and decay into f (\bar{f}) at time t is:

$$\langle f | \mathcal{H} | D^0(t) \rangle = A_f g_+(t) + \bar{A}_f \frac{q}{p} g_-(t), \quad (17)$$

$$\langle \bar{f} | \mathcal{H} | \bar{D}^0(t) \rangle = \bar{A}_{\bar{f}} g_+(t) + A_{\bar{f}} \frac{p}{q} g_-(t), \quad (18)$$

6 *Chavez, Cowan, and Lockman*

where A_f and \bar{A}_f are the D^0 and \bar{D}^0 decay amplitudes to a final state f ; $A_{\bar{f}}$ and $\bar{A}_{\bar{f}}$ are the D^0 and \bar{D}^0 decay amplitudes to a final state \bar{f} :

$$A_f \equiv \langle f | \mathcal{H} | D^0 \rangle, \quad (19)$$

$$\bar{A}_f \equiv \langle f | \mathcal{H} | \bar{D}^0 \rangle, \quad (20)$$

$$A_{\bar{f}} \equiv \langle \bar{f} | \mathcal{H} | D^0 \rangle, \quad (21)$$

$$\bar{A}_{\bar{f}} \equiv \langle \bar{f} | \mathcal{H} | \bar{D}^0 \rangle. \quad (22)$$

where \mathcal{H} is the Hamiltonian governing weak decays. Written in terms of the decay amplitudes, the general expressions for the time-dependent decay rates $\Gamma(D^0(t) \rightarrow f)$ and $\Gamma(\bar{D}^0(t) \rightarrow \bar{f})$ are:

$$\begin{aligned} \Gamma(D^0(t) \rightarrow f) = & \frac{e^{-\Gamma t}}{2} \left[|A_f|^2 [\cosh(y\Gamma t) + \cos(x\Gamma t)] + \left| \frac{q}{p} \right|^2 |\bar{A}_f|^2 [\cosh(y\Gamma t) - \cos(x\Gamma t)] \right. \\ & \left. - 2\text{Re} \left(A_f^* \bar{A}_f \frac{q}{p} \right) \sinh(y\Gamma t) + 2\text{Im} \left(A_f^* \bar{A}_f \frac{q}{p} \right) \sin(x\Gamma t) \right], \end{aligned} \quad (23)$$

$$\begin{aligned} \Gamma(\bar{D}^0(t) \rightarrow \bar{f}) = & \frac{e^{-\Gamma t}}{2} \left[|\bar{A}_{\bar{f}}|^2 [\cosh(y\Gamma t) + \cos(x\Gamma t)] + \left| \frac{p}{q} \right|^2 |A_{\bar{f}}|^2 [\cosh(y\Gamma t) - \cos(x\Gamma t)] \right. \\ & \left. - 2\text{Re} \left(\bar{A}_{\bar{f}}^* A_{\bar{f}} \frac{p}{q} \right) \sinh(y\Gamma t) + 2\text{Im} \left(\bar{A}_{\bar{f}}^* A_{\bar{f}} \frac{p}{q} \right) \sin(x\Gamma t) \right]. \end{aligned} \quad (24)$$

To describe the time dependence for the “wrong-sign” (WS) decay such as $D^0 \rightarrow K^+ \pi^-$ ($\bar{D}^0 \rightarrow K^- \pi^+$), we rewrite Eq. 23 (Eq. 24) in terms of the Cabibbo-favored (CF) amplitude \bar{A}_f ($A_{\bar{f}}$) and the parameter λ_f^{-1} ($\lambda_{\bar{f}}$), where

$$\lambda_f \equiv \frac{q}{p} \frac{\bar{A}_f}{A_f}. \quad (25)$$

For decay times t satisfying $|x\Gamma t|, |y\Gamma t| \ll 1$, the decay rates are given by:

$$\Gamma(D^0(t) \rightarrow f) = e^{-\Gamma t} |\bar{A}_f|^2 \left| \frac{q}{p} \right|^2 \left[\left| \lambda_f^{-1} \right|^2 - \text{Re} \left(\lambda_f^{-1} \right) y\Gamma t - \text{Im} \left(\lambda_f^{-1} \right) x\Gamma t + \frac{x^2 + y^2}{4} (\Gamma t)^2 \right], \quad (26)$$

$$\Gamma(\bar{D}^0(t) \rightarrow \bar{f}) = e^{-\Gamma t} |A_{\bar{f}}|^2 \left| \frac{p}{q} \right|^2 \left[\left| \lambda_{\bar{f}} \right|^2 - \text{Re} \left(\lambda_{\bar{f}} \right) y\Gamma t - \text{Im} \left(\lambda_{\bar{f}} \right) x\Gamma t + \frac{x^2 + y^2}{4} (\Gamma t)^2 \right]. \quad (27)$$

Under similar conditions, the time-dependent rates for D^0 and \bar{D}^0 decaying to a

CP -eigenstate $f = \bar{f} = f_{CP}$ can be written as:

$$\Gamma(D^0(t) \rightarrow f_{CP}) = e^{-\Gamma t} |A_{f_{CP}}|^2 \left[1 - \text{Re}(\lambda_{f_{CP}}) y \Gamma t + \text{Im}(\lambda_{f_{CP}}) x \Gamma t + |\lambda_{f_{CP}}|^2 \frac{x^2 + y^2}{4} (\Gamma t)^2 \right], \quad (28)$$

$$\Gamma(\bar{D}^0(t) \rightarrow f_{CP}) = e^{-\Gamma t} |\bar{A}_{f_{CP}}|^2 \left[1 - \text{Re}(\lambda_{f_{CP}}^{-1}) y \Gamma t + \text{Im}(\lambda_{f_{CP}}^{-1}) x \Gamma t + |\lambda_{f_{CP}}^{-1}|^2 \frac{x^2 + y^2}{4} (\Gamma t)^2 \right], \quad (29)$$

where the terms proportional to $e^{-\Gamma t}(\Gamma t)^2$ are due to mixing, those proportional to $e^{-\Gamma t}\Gamma t$ are due to the interference between mixing and decay, while those proportional to $e^{-\Gamma t}$ are due to direct decay. Fig. 4 illustrates the two interfering decay paths from an initial D^0 to a final state f .

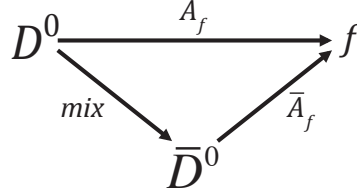


Fig. 4. Diagram illustrating the interference between the amplitude for direct D^0 decay to f and that for $D^0 \rightarrow \bar{D}^0$ mixing followed by \bar{D}^0 decay to f .

1.2. CP violation

There are three different types of CP -violating effects in meson decays:^b

- (1) CP violation (CPV) in mixing;
- (2) CPV in decay, also known as direct CPV ;
- (3) CPV in the interference between a direct decay, $D^0 \rightarrow f$, and a decay involving mixing, $D^0 \rightarrow \bar{D}^0 \rightarrow f$.

CPV in mixing and in the interference between mixing and decay is referred to as indirect CPV .

CPV in mixing occurs when the mixing probability of D^0 to \bar{D}^0 is different than the mixing probability of \bar{D}^0 to D^0 . As can be seen from Eqs. 13 and 14, this happens if and only if $|q/p| \neq 1$. This type of CP -violating effect depends only on the mixing parameters and not the final state of the decay.

As an example, consider the decay $D^0 \rightarrow K^{(*)+} l^- \bar{\nu}_l$. The diagram for this decay is illustrated in Fig. 5. Within the SM, the D^0 must first mix to \bar{D}^0 , followed by

^bFor a complete review, see Refs. 17, 20, 21.

8 *Chavez, Cowan, and Lockman*

the direct decay $\bar{D}^0 \rightarrow K^{(*)+} l^- \bar{\nu}_l$. There is no direct decay of D^0 to the final state $K^{(*)+} l^- \bar{\nu}_l$ in the SM. Therefore, the time-dependent CP asymmetry:

$$\mathcal{A}_{SL} = \frac{d\Gamma/dt(D^0 \rightarrow K^{(*)+} l^- \bar{\nu}_l) - d\Gamma/dt(\bar{D}^0 \rightarrow K^{(*)-} l^+ \nu_l)}{d\Gamma/dt(D^0 \rightarrow K^{(*)+} l^- \bar{\nu}_l) + d\Gamma/dt(\bar{D}^0 \rightarrow K^{(*)-} l^+ \nu_l)} \quad (30)$$

is equal to the mode-independent quantity:

$$A_M = \frac{|q/p|^2 - |p/q|^2}{|q/p|^2 + |p/q|^2} \quad (31)$$

which is used to characterize CPV in mixing. The techniques used to analyze the decay $D^0 \rightarrow K^{(*)+} l^- \bar{\nu}_l$ for D^0 - \bar{D}^0 mixing are discussed in Sec. 2.3.4; the results are presented in Sec. 3.3.4.

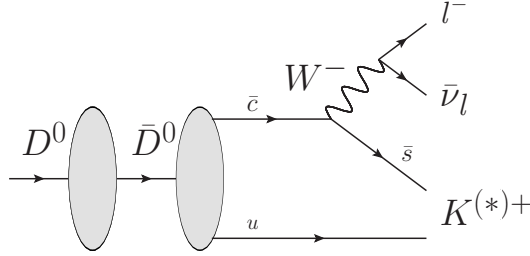


Fig. 5. Diagram for the decay $D^0 \rightarrow K^{(*)+} l^- \bar{\nu}_l$.

CPV in decay occurs when the amplitude for a decay and its CP conjugate process have different magnitudes: $|\bar{A}_{\bar{f}}/A_f| \neq 1$. In charged D modes where no mixing can occur, CPV in decay is characterized by non-zero values for the time-integrated asymmetry:

$$\mathcal{A}_{f\pm} \equiv \frac{\Gamma(D^- \rightarrow f^-) - \Gamma(D^+ \rightarrow f^+)}{\Gamma(D^- \rightarrow f^-) + \Gamma(D^+ \rightarrow f^+)} = \frac{|\bar{A}_{f-}/A_{f+}|^2 - 1}{|\bar{A}_{f-}/A_{f+}|^2 + 1} \quad (32)$$

Consider the case where two amplitudes:

$$\begin{aligned} A_f &= |a_1|e^{i(\delta_1+\phi_1)} + |a_2|e^{i(\delta_2+\phi_2)} \\ \bar{A}_{\bar{f}} &= |a_1|e^{i(\delta_1-\phi_1)} + |a_2|e^{i(\delta_2-\phi_2)} \end{aligned} \quad (33)$$

mediate the decay, where $\delta_{1,2}$ and $\phi_{1,2}$ are the strong and weak phases, respectively, of amplitude $A_{1,2}$. The weak phase changes sign under CP , whereas the strong phase does not. The CP asymmetry $\mathcal{A}_{f\pm}$ can then be written as:

$$\mathcal{A}_{f\pm} = -\frac{2|a_1||a_2|\sin(\delta_2 - \delta_1)\sin(\phi_2 - \phi_1)}{|a_1|^2 + |a_2|^2 + 2|a_1||a_2|\cos(\delta_2 - \delta_1)\cos(\phi_2 - \phi_1)}. \quad (34)$$

Thus, direct CPV will occur ($\mathcal{A}_{f\pm} \neq 0$) only if the differences between the CP -conserving strong phases and the differences between the CP -violating weak phases

of the two contributing amplitudes are not zero or multiples of π . In neutral D decays, direct CPV is characterized by the mode-dependent parameter A_D :¹⁹

$$A_D \equiv \frac{|A_f/\bar{A}_f|^2 - |\bar{A}_f/A_f|^2}{|A_f/\bar{A}_f|^2 + |\bar{A}_f/A_f|^2}. \quad (35)$$

CPV in the interference between a decay without mixing, $D^0 \rightarrow f$, and a decay with mixing, $D^0 \rightarrow \bar{D}^0 \rightarrow f$, where f can be reached from both D^0 and \bar{D}^0 decays, can also occur. Consider the time-dependent rate asymmetry of neutral meson decays to a final CP eigenstate:

$$A_{CP}(t) = \frac{\Gamma(D^0(t) \rightarrow f_{CP}) - \Gamma(\bar{D}^0(t) \rightarrow f_{CP})}{\Gamma(D^0(t) \rightarrow f_{CP}) + \Gamma(\bar{D}^0(t) \rightarrow f_{CP})} \quad (36)$$

If both CPV in mixing and decay are absent, then $|q/p| = 1$, $|\bar{A}_{f_{CP}}/A_{f_{CP}}| = 1$ and therefore, $|\lambda_{f_{CP}}| = 1$. As can be seen by comparing Eqs. 28 and 29, $A_{CP}(t)$ will be nonzero when $\lambda_{f_{CP}}^{-1} \neq \lambda_{f_{CP}}$. Therefore, CPV in the interference between mixing and decay will be present if $\text{Im}\lambda_{f_{CP}} \neq 0$, which implies $\sin \phi_{f_{CP}} \neq 0$, where $\lambda_{f_{CP}} \equiv |\lambda_{f_{CP}}| \exp(i\phi_{f_{CP}})$. The phase $\phi_{f_{CP}}$ is the sum of the phase difference between q and p ,

$$\varphi \equiv \arg(q/p) \quad (37)$$

and the (weak) phase difference between \bar{A}_f and A_f . In general, the weak phase component of $\arg(\lambda_f)$ is said to characterize CPV in the interference between mixing and decay.

The quantities λ_f^{-1} and $\lambda_{\bar{f}}$ can be evaluated for the modes $f = K^+\pi^-$ and $f = K^+K^-$ in terms of A_M and the mode-dependent quantities R_D , A_D , A_D^{KK} , $\phi_{K\pi}$ and ϕ_{KK} :¹⁹

$$\lambda_{K^+\pi^-}^{-1} = -\sqrt{R_D} \sqrt[4]{\frac{(1+A_D)(1-A_M)}{(1-A_D)(1+A_M)}} e^{-i(\delta_{K\pi} + \phi_{K\pi})}, \quad (38)$$

$$\lambda_{K^-\pi^+} = -\sqrt{R_D} \sqrt[4]{\frac{(1-A_D)(1+A_M)}{(1+A_D)(1-A_M)}} e^{-i(\delta_{K\pi} - \phi_{K\pi})}, \quad (39)$$

$$\lambda_{K^+K^-} = \sqrt[4]{\frac{(1-A_D^{KK})(1+A_M)}{(1+A_D^{KK})(1-A_M)}} e^{i\phi_{KK}}. \quad (40)$$

For $f = K^+\pi^-$ the quantity R_D is defined to be

$$R_D \equiv \sqrt{R_D^+ R_D^-}, \quad R_D^+ \equiv |A_{K^+\pi^-}/\bar{A}_{K^+\pi^-}|^2, \quad R_D^- \equiv |\bar{A}_{K^-\pi^+}/A_{K^-\pi^+}|^2. \quad (41)$$

In the absence of direct CPV ,

$$R_D^+ = |A_{K^+\pi^-}/A_{K^-\pi^+}|^2, \quad R_D^- \equiv |\bar{A}_{K^-\pi^+}/\bar{A}_{K^+\pi^-}|^2, \quad (42)$$

are the ratios of the doubly-Cabibbo-suppressed (DCS) to Cabibbo-favored (CF) decay widths for D^0 and \bar{D}^0 decays, respectively. These ratios are $\mathcal{O}(\tan^4(\theta_c)) \approx 0.3\%$,

where θ_c is the Cabibbo angle. Additionally, $\delta_{K\pi}$ is the relative strong phase between $A_{K^+\pi^-}$ and $\bar{A}_{K^+\pi^-}$. The quantities A_D and ϕ are in general mode-dependent. However, assuming that SM tree-level amplitudes dominate the decays, ϕ appearing in Eqs. 38, 39 and 40 will be the same for the $K\pi$ and KK modes.^{21,22}

Traditional SM estimates for CP asymmetries in D -meson decays are small, less than $\mathcal{O}(0.01\%)$.^{23,24,25} This is because, to a very good approximation, only two generations of quarks are involved in charm mixing and decay, while the CKM mechanism²⁶ requires three quark generations to produce CPV .²⁷ Present experimental uncertainties on time-integrated CP asymmetries in D decays are $\mathcal{O}(0.1\%)$.¹⁵ Through 2010, all measured CP asymmetries in D decays were consistent with zero within experimental errors.^{15,19}

In 2011, the LHCb Collaboration presented evidence for direct CPV by measuring the difference in time-integrated CP asymmetries between two singly Cabibbo suppressed D decay modes: $\Delta A_{CP} \equiv A_{CP}(D \rightarrow K^+K^-) - A_{CP}(D \rightarrow \pi^+\pi^-) = (-0.82 \pm 0.21(\text{stat}) \pm 0.11(\text{syst}))\%$.²⁸ In this difference, the mode-independent indirect contribution cancels. A new standard model calculation²⁹ of this difference, while uncertain to a factor of a few, may accommodate this intriguingly large experimental result. New physics, such as supersymmetric gluino-squark loops, could also yield direct CP asymmetries as large as $\mathcal{O}(1\%)$.³⁰

1.3. Outline

This paper discusses the experimental status of D^0 - \bar{D}^0 mixing and CPV as of the end of the 2011 calendar year. We review the current results from recent colliding-beam and fixed-target experiments and discuss in some detail the techniques involved. We survey the primary analysis methods used to study two-body and multi-body hadronic and semileptonic D^0 decays. Then we present results from experimental measurements of mixing and searches for CPV from time-independent analyses (those that do not use the proper decay time of the D^0 to search for mixing) and time-dependent analyses (which do use the proper D^0 decay time) as well as quantum-correlated decays. Finally we review future prospects for measurements in the near- and longer-term future and summarize the overall status of D^0 - \bar{D}^0 mixing experiments.

2. Analysis Techniques for Measuring Charm Mixing and CP Violation

2.1. Time-independent Methods

Time-independent methods provide an important technique for measuring D^0 - \bar{D}^0 mixing and searching for CP violation in charm decays. They also yield information on relative strong phases between mixed and direct decays for several different hadronic modes of interest to mixing studies. Knowledge of the strong phase $\delta_{K\pi}$ between $D^0 \rightarrow K^+\pi^-$ and $\bar{D}^0 \rightarrow K^+\pi^-$ allows conversion of the observable y' to mixing parameter y (see Sec. 2.2.1).

As the name implies, these methods do not make use of decay-time information. Instead, they count the numbers of D^0 and \bar{D}^0 decays to specific modes when the $D^0\bar{D}^0$ pair has been produced in a quantum-coherent, charge conjugation (C) eigenstate. Relative numbers of decay modes of both singly-tagged (ST) events, where one D^0 or \bar{D}^0 is fully reconstructed, and doubly-tagged (DT) events, where both the D^0 and the \bar{D}^0 mesons are fully reconstructed, provide information on the mixing parameters x and y , the strong phase differences δ_i for each decay mode i , and their DCS decay rates. This method is especially useful when separating the individual D^0 and \bar{D}^0 decay vertices is difficult, as in the case of non-asymmetric energy e^+e^- colliders.

At present, these methods have been performed^{31,32} only at the 3.770 GeV resonance, but could also be done at higher center-of-mass energies through initial-state radiation, if the number of ISR photons can be determined (so that the CP state of the coherent $D^0\bar{D}^0$ pair is known).

2.1.1. Correlated Decays at 3.770 GeV

In e^+e^- collisions at or above 3.770 GeV that produce a $D^0\bar{D}^0$ pair, the production of the pair may be assumed to proceed through a single virtual photon with $J^{PC} = 1^{--}$. At 3.770 GeV, the final state will have $C = -1$. At higher energies, additional pions and photons may be produced:³³

$$e^+e^- \rightarrow D^0\bar{D}^0 + m(\pi^0) + n(\gamma) \quad (43)$$

where $m, n \geq 0$. Therefore the $D^0\bar{D}^0$ pair will be produced with $C(D^0\bar{D}^0) = -1^{n+1}$. When $n = 0$, $C(D^0\bar{D}^0)$ will be -1 . The value of m is not a factor since $C(\pi^0) = +1$.

Additionally, if the $D^0\bar{D}^0$ pair has relative angular momentum l , then $C(D^0\bar{D}^0) = P(D^0\bar{D}^0) = -1^l$ where P is the parity operator. Assuming CP is conserved, we can write the wavefunction of the $D^0\bar{D}^0$ state in the center of mass system (where the mesons have momentum \vec{p} and $-\vec{p}$, respectively) in terms of either the flavor eigenstates D^0 and \bar{D}^0 or the CP eigenstates D_1, D_2 (with $CP = +1, -1$ respectively). If n is even ($0, 2, \dots$), the produced $D^0\bar{D}^0$ state is

$$|D^0(\vec{p})\rangle|\bar{D}^0(-\vec{p})\rangle - |\bar{D}^0(\vec{p})\rangle|D^0(-\vec{p})\rangle = |D_2(\vec{p})\rangle|D_1(-\vec{p})\rangle - |D_1(\vec{p})\rangle|D_2(-\vec{p})\rangle \quad (44)$$

which has $C = P = -1$. If n is odd, the produced state is

$$|D^0(\vec{p})\rangle|\bar{D}^0(-\vec{p})\rangle + |\bar{D}^0(\vec{p})\rangle|D^0(-\vec{p})\rangle = |D_1(\vec{p})\rangle|D_1(-\vec{p})\rangle - |D_2(\vec{p})\rangle|D_2(-\vec{p})\rangle \quad (45)$$

with $C = P = +1$. Therefore at 3.770 GeV when both the D^0 and \bar{D}^0 decay to CP -eigenstates, they will have opposite CP . If any same- CP decays occur, the number produced will be a measure of the rate of charm mixing.

To connect the number of like- CP and opposite- CP events to the mixing rate and strong phase δ_i for a given decay mode i , expressions for time-integrated rates for ST or DT events can be calculated from decay amplitudes. Observed rates for one or

more modes can be investigated simultaneously, with mixing parameters and strong phases obtained from a simultaneous fit to all decay modes under consideration.

As an example, consider the DT decay to $(K^- \pi^+, K^- \pi^+)$. From a $CP = -1$ $D^0 \bar{D}^0$ coherent state, this rate should be zero in the absence of mixing. A short calculation³⁴ yields

$$\Gamma^{(CP=-1)}(K^- \pi^+, K^- \pi^+) = \frac{1}{2} |A_{K^- \pi^+}|^4 \left| 1 - r_{K\pi}^2 e^{-2i\delta'_{K\pi}} \right|^2 (x^2 + y^2) \quad (46)$$

$$\approx \frac{1}{2} |A_{K^- \pi^+}|^4 (x^2 + y^2), \quad (47)$$

where $A_{K\pi} = \langle K^- \pi^+ | D^0 \rangle$, $\bar{A}_{K\pi} = \langle K^- \pi^+ | \bar{D}^0 \rangle$, $r_{K\pi} \equiv |\bar{A}_{K\pi}/A_{K\pi}|$, and $\delta'_{K\pi}$ is the strong phase difference between $\bar{A}_{K\pi}$ and $A_{K\pi}$:

$$\bar{A}_{K\pi}/A_{K\pi} \equiv r_{K\pi} e^{-i\delta'_{K\pi}} = -r_{K\pi} e^{-i(\delta_{K\pi} + \pi)}, \quad (48)$$

where we have incorporated the phase convention used by CLEO in the definition of $\delta'_{K\pi}$. Note that if the mixing rate $R_M \equiv (x^2 + y^2)/2$ vanishes, then $\Gamma^{(CP=-1)}(K^- \pi^+, K^- \pi^+)$ will vanish. A non-zero rate will be an indication of the presence of mixing. This rate can be contrasted with the DT $(K^- \pi^+, K^+ \pi^-)$ decay rate

$$\Gamma^{(CP=-1)}(K^- \pi^+, K^+ \pi^-) = |A_{K^- \pi^+}|^4 \left| 1 - r_{K\pi}^2 e^{-2i\delta'_{K\pi}} \right|^2 \left[1 - \frac{1}{2}(x^2 - y^2) \right] \quad (49)$$

$$\approx |A_{K^- \pi^+}|^4 \left[1 - 2r_{K\pi}^2 \cos 2\delta'_{K\pi} - \frac{1}{2}(x^2 - y^2) \right]. \quad (50)$$

Comparison of these rates yields information on $R_M \equiv (x^2 + y^2)/2$. Inclusion of other DT decay mode pairs permits measurement of x , y , δ_i , and D^0 branching fractions. See Table 1.

D^0 final states used by CLEO-c³¹ are $K^\pm \pi^\mp$, $K^+ K^-$, $\pi^+ \pi^-$, $K_s^0 \pi^0 \pi^0$, $K_L^0 \pi^0$, $K_s^0 \pi^0$, $K_s^0 \eta$, $K_s^0 \omega$, and inclusive semileptonic decays $X e^+ \nu_e$, $X e^- \bar{\nu}_e$. Events containing neutral D candidates are selected using two quantities, the beam-constrained mass M :

$$M \equiv \sqrt{E_0^2 - \vec{p}_D^2/c^2} \quad (51)$$

and the energy difference $\Delta E \equiv E_D - E_0$ where E_0 is the beam energy, E_D is the sum of energies of the D^0 candidate decay products, and \vec{p}_D is the D^0 candidate momentum. Well-reconstructed D^0 candidates will have distributions that peak at the D^0 mass in M and at zero in ΔE . After mode-dependent cuts on ΔE are imposed, ST yields are obtained by fitting the M distribution and DT yields by counting events in a signal region in the two-dimensional M distribution.

Semileptonic decays are reconstructed inclusively, with only the electron required to be identified. Electron identification is performed by use of multivariate techniques.³⁶ Decays involving K_L^0 mesons or neutrinos are reconstructed using a missing-mass technique only in DT events.³⁷

Table 1. Correlated and uncorrelated decay rates for ST and DT events used in analysis of coherent $D^0\bar{D}^0$ decays by CLEO-c.^{31,35} Rates are normalized to the branching fraction(s) of reconstructed mode(s) (note that a normalization is used where A_j^2 is the D^0 branching fraction to mode j when no mixing is present). $S_+(S_-)$ denotes a decay to a $CP = +1(-1)$ eigenstate; e^- denotes a semileptonic decay containing e^- . Rates are given to leading order in x , y , and R_{WS} , the WS-to-RS decay rate ratio. Effects of CP violation are negligible. Charge-conjugate modes are implied.

ST mode	Uncorrelated rate	Correlated rate
$K^-\pi^+$	$1 + R_{WS}$	$1 + R_{WS}$
S_\pm	2	2
DT mode	Uncorrelated rate	Correlated rate
$K^-\pi^+, K^-\pi^+$	R_{WS}	R_M
$K^-\pi^+, K^+\pi^-$	$1 + R_{WS}^2$	$(1 + R_{WS})^2 - 4r \cos \delta_{K\pi} (r \cos \delta_{K\pi} + y)$
$K^-\pi^+, S_\pm$	$1 + R_{WS}$	$1 + R_{WS} \pm 2r \cos \delta_{K\pi} \pm y$
$K^-\pi^+, e^-$	1	$1 - ry \cos \delta_{K\pi} - rx \sin \delta_{K\pi}$
S_\pm, S_\pm	1	0
S_+, S_-	2	4
S_\pm, e^-	1	$1 \pm y$

Measurements of x^2 , y , r^2 , $rx \sin \delta_{K\pi}$, and $r \cos \delta_{K\pi}$ are obtained from the observed ST and DT yields and external branching fraction measurements using a least-squares fit.³⁸ The DT yields provide information on mixing and strong phase parameters. Use of ST and DT yields simultaneously provides normalization, so that independent measurements of the absolute $D^0\bar{D}^0$ production rate and the integrated luminosity are not required. This method is described fully in Refs. 35, 39, and 40, including event selection and global fit techniques. Quantum-correlated results are presented in Section 3.1.1.

2.2. Time-dependent Analyses of Two-body Decays

2.2.1. $D^0 \rightarrow K^+\pi^-$ Wrong-sign Analysis

In the wrong-sign (WS) D^0 decay, $D^0 \rightarrow K^+\pi^-$, the $K^+\pi^-$ final state may be reached either through a direct, doubly Cabibbo-suppressed (DCS) decay, or through mixing, $D^0 \rightarrow \bar{D}^0$, followed by the Cabibbo-favored (CF) right-sign (RS) decay, $\bar{D}^0 \rightarrow K^+\pi^-$. Since the two processes involve the same initial- and final states and are therefore indistinguishable, interference between the two amplitudes will occur. For D^0 decays to $K^+\pi^-$ and \bar{D}^0 decays to $K^-\pi^+$, we define the WS decay rates relative to the RS decay rates as follows:

$$R_{WS}^+(t) \equiv \frac{\Gamma(D^0(t) \rightarrow K^+\pi^-)}{e^{-\Gamma t} |\bar{A}_{K^+\pi^-}|^2}, \quad R_{WS}^-(t) \equiv \frac{\Gamma(\bar{D}^0(t) \rightarrow K^-\pi^+)}{e^{-\Gamma t} |A_{K^-\pi^+}|^2}. \quad (52)$$

From Eqs. 26, 27, 38 and 39 these are given by:

$$R_{WS}^\pm(t) = R_D^\pm + y'^\pm \sqrt{R_D^\pm}(\Gamma t) + \frac{x'^{\pm 2} + y'^{\pm 2}}{4}(\Gamma t)^2, \quad (53)$$

where the mixing parameters x'^+, y'^+ (x'^-, y'^-):

$$x'^{\pm} \equiv \sqrt[4]{\frac{1 \pm A_M}{1 \mp A_M}} [x' \cos \phi \pm y' \sin \phi], \quad (54)$$

$$y'^{\pm} \equiv \sqrt[4]{\frac{1 \pm A_M}{1 \mp A_M}} [y' \cos \phi \mp x' \sin \phi]. \quad (55)$$

are the mixing parameters measured in the D^0 (\bar{D}^0) decay modes, ϕ is the weak phase characterizing CPV in the interference between mixing and decay, and the parameters x' and y' are related to the mixing parameters x and y through a rotation by the strong phase, $\delta_{K\pi}$:

$$x' \equiv x \cos \delta_{K\pi} + y \sin \delta_{K\pi}, \quad (56)$$

$$y' \equiv y \cos \delta_{K\pi} - x \sin \delta_{K\pi}. \quad (57)$$

The DCS branching fraction for D^0 and \bar{D}^0 decays is related to the direct CPV asymmetry parameter A_D as follows:

$$R_D^{\pm} \equiv R_D \sqrt{\frac{1 \pm A_D}{1 \mp A_D}}. \quad (58)$$

In the limit of CP conservation ($A_D = A_M = \phi = 0$), Eq. 53 reduces to:

$$R_{WS}(t) = R_D + y' \sqrt{R_D} (\Gamma t) + \frac{x'^2 + y'^2}{4} (\Gamma t)^2. \quad (59)$$

The relative WS decay rate allows a determination of x'^2 , y' and R_D , but not the strong phase $\delta_{K\pi}$. For small mixing parameter values, the main sensitivity to mixing comes through the interference term which is linear in $y'\Gamma t$. Tree diagrams for the two amplitudes mediating the $D^0 \rightarrow K^+\pi^-$ decay are shown in Fig. 6.

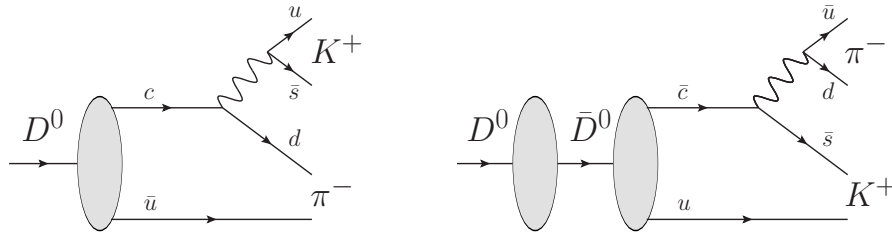


Fig. 6. Diagrams illustrating two ways to reach the $K^+\pi^-$ final state from an initial D^0 . Left: direct DCS decay, $D^0 \rightarrow K^+\pi^-$. Right: mixing, $D^0 \rightarrow \bar{D}^0$, followed by CF decay, $\bar{D}^0 \rightarrow K^+\pi^-$.

Experiments use the slow pion π_s^+ in the strong decay $D^{*+} \rightarrow \pi_s^+ D^0$ to tag the charm flavor of the neutral D at production.^c The charge of the π_s ,

^cUnless otherwise stated, reference to a given decay mode implies reference to its CP -conjugate mode as well.

together with the charge of the kaon from the decay of the neutral D allows the signal sample to be divided into four categories: two WS decay samples, $D^{*+} \rightarrow \pi_s^+ D^0$, $D^0 \rightarrow K^+ \pi^- + c.c.$, and two much larger right-sign (RS) decay control samples, $D^{*+} \rightarrow \pi_s^+ D^0$, $D^0 \rightarrow K^- \pi^+ + c.c.$. A simultaneous fit to the RS and WS distributions is performed to determine the direct CF and DCS lifetime and the parameters of the decay-time resolution model (from the RS and WS samples) and the parameters R_D , x'^2 , y' (from the WS sample). The independent variables of the fit are $m_{K\pi}$, the reconstructed $K\pi$ invariant mass; Δm , the $D^{*+}-D^0$ mass difference; t , the reconstructed decay time, and its measured uncertainty, σ_t . The variables $m_{K\pi}$ and Δm are used to separate signal from background. At *BABAR*, the vertical height of the beam spot is $\approx 6 \mu\text{m}$. This beam spot information is used to constrain the location of the D^* vertex, thus substantially improving the determination of Δm and the reconstructed decay time, t . Fig. 7 shows the projections of the $m_{K\pi}$ and Δm data and signal and background fit functions from the 2007 384 fb^{-1} WS *BABAR* data set.¹²

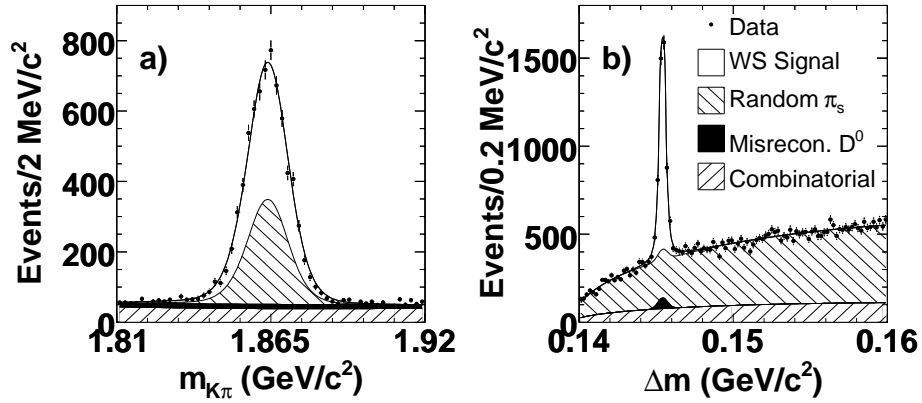


Fig. 7. *BABAR* distributions of (a): $m_{K\pi}$ from WS candidates with $0.1445 < \Delta m < 0.1465 \text{ GeV}/c^2$ and (b): Δm for WS candidates with $1.843 < m_{K\pi} < 1.883 \text{ GeV}/c^2$. The projections of the signal- and background fits are overlaid, where the random π_s background sample peaks in $m_{K\pi}$ but not in Δm ; the misreconstructed D^0 paired with a π_s from a D^* peaks in Δm but not in $m_{K\pi}$; the combinatoric background sample peaks neither in $m_{K\pi}$ nor in Δm . Reprinted figure with permission from B. Aubert *et al.*, *Phys. Rev. Lett.* 98, 211802 (2007). Copyright 2007 by the American Physical Society.¹²

2.2.2. D^0 Lifetime Ratio Analysis

In this section we describe analysis techniques which measure the decay-time distributions of neutral D mesons decaying to CP eigenstates and CP mixed states. The potential of this method was first described in Ref. 41, and the first experimental results were presented utilizing these techniques in Ref. 42. In the last ten years,

several experimental collaborations have measured $D^0\bar{D}^0$ mixing and CP violation observables with increasing precision by comparing the rate for D^0 mesons decaying to flavor-specific final states.

In particular, the mixing parameter y (Eq. 2) may be measured by comparing the rate of D^0 decays to CP eigenstates with decays to non- CP eigenstates. If decays to CP eigenstates have a shorter effective lifetime than those decaying to non- CP eigenstates, then y is positive.

Experimentally, one is interested in collecting high purity samples with large statistics of D^0 decays to final states of specific CP content. The two-body SM processes with these characteristics are the singly-Cabibbo-suppressed decays to CP -even eigenstates, $D^0 \rightarrow K^+ K^-$ and $D^0 \rightarrow \pi^+ \pi^-$, shown in Figs. 8(a) and 8(b) respectively, and the Cabibbo-favored decay to CP -mixed final state, $D^0 \rightarrow K^- \pi^+$, shown in Fig. 9, and the corresponding CP -conjugate decay processes.

Similarly to the two-body final states, the mixing parameter y can also be measured by analyzing the CP -odd component of $D^0 \rightarrow K_s^0 K^+ K^-$ decays, by means of comparing the mean decay times for different regions of the three-body phase space distribution of the final state.^d

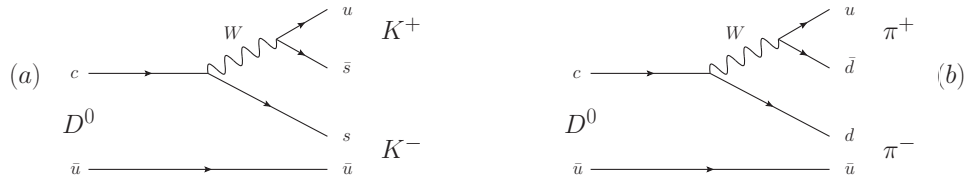


Fig. 8. Feynman diagrams for singly-Cabibbo-suppressed decays of D^0 to CP eigenstates, $D^0 \rightarrow K^+ K^-$ (a), and $D^0 \rightarrow \pi^+ \pi^-$ (b).

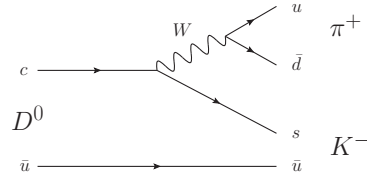


Fig. 9. Feynman diagram of the Cabibbo-favored decay $D^0 \rightarrow K^- \pi^+$.

^dDetails of this measurement will be discussed in Sec. 2.3.

Neglecting the quadratic (mixing) terms in Eqs. 28 and 29, an approximation valid when $|\lambda_{f_{CP}}| \approx 1$ and $|x\Gamma t|, |y\Gamma t| \ll 1$, we obtain the the following expressions for the time-dependent decay rates $\Gamma(D^0(t) \rightarrow h^+h^-)$ and $\Gamma(\bar{D}^0(t) \rightarrow h^+h^-)$:

$$\begin{aligned}\Gamma(D^0(t) \rightarrow h^+h^-) &= e^{-\Gamma t} |A_{h^+h^-}|^2 \{1 - [\text{Re}(\lambda_{h^+h^-})y - \text{Im}(\lambda_{h^+h^-})x]\Gamma t\}, \\ \Gamma(\bar{D}^0(t) \rightarrow h^+h^-) &= e^{-\Gamma t} |\bar{A}_{h^+h^-}|^2 \{1 - [\text{Re}(\lambda_{h^+h^-}^{-1})y - \text{Im}(\lambda_{h^+h^-}^{-1})x]\Gamma t\},\end{aligned}\quad (60)$$

$$\begin{aligned}\Gamma(D^0(t) \rightarrow K^-\pi^+) &= e^{-\Gamma t} |A_{K^-\pi^+}|^2, \\ \Gamma(\bar{D}^0(t) \rightarrow K^+\pi^-) &= e^{-\Gamma t} |\bar{A}_{K^+\pi^-}|^2,\end{aligned}\quad (61)$$

where $h = \pi, K$. In the absence of direct CP violation (as expected in the SM), but allowing for a small indirect CP violation (with a weak phase $|\phi| \ll 1$), we can write $\lambda_{h^+h^-} = |q/p| e^{i\phi}$. To a good approximation, these decay-time distributions can be treated as exponentials with effective lifetimes given by Ref. 43

$$\begin{aligned}\tau_{K\pi} &= \tau(D^0 \rightarrow K^-\pi^+) = \tau(\bar{D}^0 \rightarrow K^+\pi^-), \\ \tau_{hh}^+ &= \tau(D^0 \rightarrow h^+h^-) = \tau_{K^-\pi^+} \left[1 + \left|\frac{q}{p}\right| (y \cos \phi - x \sin \phi)\right]^{-1}, \\ \tau_{hh}^- &= \tau(\bar{D}^0 \rightarrow h^+h^-) = \tau_{K^-\pi^+} \left[1 + \left|\frac{p}{q}\right| (y \cos \phi + x \sin \phi)\right]^{-1},\end{aligned}\quad (62)$$

as before $h = \pi, K$. Combining these quantities we then define the parameters y_{CP} , A_Γ and ΔY as:

$$\begin{aligned}y_{CP} &= \frac{\tau_{K\pi}}{\langle \tau_{hh} \rangle} - 1, \\ A_\Gamma &= \frac{\tau(\bar{D}^0 \rightarrow h^-h^+) - \tau(D^0 \rightarrow h^+h^-)}{\tau(\bar{D}^0 \rightarrow h^-h^+) + \tau(D^0 \rightarrow h^+h^-)}, \\ \Delta Y &= \frac{\tau_{K\pi}}{\langle \tau_{hh} \rangle} A_\Gamma,\end{aligned}$$

where $\langle \dots \rangle$ implies average over flavors, $\langle \tau_{hh} \rangle = (\tau_{hh}^+ + \tau_{hh}^-)/2$ and $h = \pi, K$. In the limit of CP conservation, $y_{CP} = y$ and $\Delta Y = 0$. In the absence of D^0 - \bar{D}^0 mixing, both y_{CP} and ΔY are zero.

Measurements of y_{CP} have been conducted at e^+e^- colliders (*BABAR*, *Belle* and *CLEO*) as well as fixed-target experiments (*FOCUS* and *E791*). Historically, experiments at e^+e^- colliders have relied on the kinematic separation of charm decays at high center-of-mass momentum (from $e^+e^- \rightarrow c\bar{c}$) to reduce backgrounds. In addition, excellent particle identification and tracking capabilities for hadrons over a large range of momenta are required when measuring y_{CP} .

The *BABAR* and *Belle* experiments have both produced measurements of y_{CP} and A_Γ ^{13,44,45} by means of selecting highly pure samples with high statistics of D^0 candidates decaying to K^+K^- , $\pi^+\pi^-$ and $K^-\pi^+$ final states, as shown in Fig. 10. In these experiments, D mesons are produced from $c\bar{c}$ initial states and as secondaries from B decays, those produced from $c\bar{c}$ events are used in the lifetime ratio measurements by choosing high momentum D mesons as well as minimizing other backgrounds. However, slightly different strategies were followed by different experiments, but the description of what follows is in general correct for all y_{CP}

measurements. We focus primarily on the measurements done at the B -factories as those are the most precise.

The so-called tagged technique is implemented by reconstructing $D^{*\pm} \rightarrow D^0 \pi_s^\pm$ decays, where the slow π_s^\pm determines the flavor of the decaying neutral meson as D^0 or \bar{D}^0 at creation. The D^0 candidates are selected by kinematically combining pairs of oppositely-charged K^\pm and π^\pm tracks that have a common vertex, and have an invariant mass typically in the range between 1.8 GeV and 1.92 GeV (approximately ± 60 MeV around the nominal D^0 mass¹⁹). The kinematic fit provides the D^0 decay position and its momentum vector p_{D^0} , which is required to point back to the e^+e^- interaction region. The D^0 candidate and the slow π_s^\pm are also required to form a common vertex in the interaction region. For each D^0 candidate the proper decay time t and its error σ_t are calculated using the decay length $l = \beta\gamma ct = ctp_{D^0}/m_{D^0}$.

To further suppress background events, Belle exploits the distribution of the energy released in the $D^{*\pm}$ decay given by $Q = m_{D^*} - m_{D^0} - m_\pi$; equivalently, BABAR uses the distribution of the mass difference Δm of the reconstructed $D^{*\pm}$ and the D^0 candidates in the event. Typically D^0 candidates are required to be within ± 0.1 MeV of the peak of the Δm or Q distributions.

The BABAR D^0 invariant mass distribution of tagged events of different decay channels are shown in Fig. 10.⁴⁴ The shaded area shows the sample of events used in the lifetime measurements. These events were selected after particle identification, tracking, and vertex probability requirements.

In the tagged sample, the charge of the reconstructed $D^{*\pm}$ allows the determination of the lifetime separately for D^0 or \bar{D}^0 decays. The lifetimes are determined by performing a simultaneous maximum likelihood fit to the reconstructed decay time and its error to all five decay samples ($D^0 \rightarrow K^-\pi^+$ and $\bar{D}^0 \rightarrow K^+\pi^-$ decay samples are combined into one). In general, there are three main PDF components entering the lifetime fit: signal, combinatoric background, and misreconstructed charm decays.

In the so-called untagged technique, there is no reconstructed $D^{*\pm}$, hence it is not possible to identify the initial flavor of the decaying D^0 meson. In the untagged analysis, the D^0 may be produced directly from a $c\bar{c}$ state or as a decay product of a higher mass resonance (other than $D^{*\pm}$). The D^0 momentum is required to point back to the beam spot in order to reduce backgrounds. In order to exclude D^0 mesons coming from B decays, D^0 candidates with momentum in the e^+e^- center-of-mass (CM) frame less than 2.5 GeV/c.

In the untagged BABAR analysis,⁴⁵ all events appearing in the tagged data sample are removed from the untagged sample in order to treat the tagged and untagged results as statistically independent from one another. The signal yields in the untagged data samples are about 3.5 times larger than those in the respective tagged samples; however, their purity is lower and the systematic uncertainties due to the higher backgrounds are more challenging.

The signal PDF is generally described by an exponential convolved with a resolution function, which is composed of three Gaussian functions sharing some common

parameters between them. The high statistics of the Cabibbo-favored $D^0 \rightarrow K^- \pi^+$ sample drives the determination of the resolution function parameters in the lifetime fit. In the tagged analysis, the random combinatoric background in the signal region is determined from a sideband region in D^0 invariant mass (m_{D^0}) and Δm . In the untagged analysis, two sideband regions in m_{D^0} are defined, one above the D^0 mass peak and one below. A small background component corresponding to misreconstructed charm decays that have long lifetimes and can thus mimic the decay time of signal events is included. The proper time distribution for this background is taken from Monte Carlo (MC).

While systematic uncertainties are expected to cancel in the lifetime ratio, the sources of backgrounds are different for each final state, hence systematics from background sources are not necessarily expected to cancel. The main signal model systematic uncertainties are the selection of the D^0 invariant mass signal region window (central position and size), opening angle distributions, and variations of the signal resolution model. The systematic uncertainties associated with backgrounds are the combinatorial PDF model and its normalization, and the misreconstructed charm PDF model (taken from simulation) and its normalization.

Results from these measurements are discussed in section 3.2.2 below.

2.3. Time-dependent Analyses of Hadronic Multi-body Decay Modes

Amplitude analyses of multi-body D^0 decay modes provide what are potentially the most definitive measurements of charm mixing parameters. Advantages include the ability, for some decay modes, to measure mixing without the ambiguity of an unknown strong phase or insensitivity to the sign of x' that limits the measurement to x'^2 and y' rather than x and y , as is the case with the time-dependent analysis of $D^0 \rightarrow K^+ \pi^-$ decays. Multi-body decays useful in this regard include $D^0 \rightarrow K_s^0 K^+ K^-$ or $K_s^0 \pi^+ \pi^-$, which we will generically designate as $K_s^0 h^+ h^-$ where h represents K or π . Three-body decays also include $D^0 \rightarrow K^+ \pi^- \pi^0$. Four-body decays include $D^0 \rightarrow K^+ \pi^- \pi^+ \pi^-$. Three-body decays are amenable to “Dalitz-plot analysis,” while higher-order decays require other methods.

2.3.1. $D^0 \rightarrow K_s^0 h^+ h^-$ Analysis

BABAR, *Belle*, and *CLEO* have performed studies of D^0 - \bar{D}^0 mixing using the decays $D^0 \rightarrow K_s^0 \pi^+ \pi^-$, $D^0 \rightarrow K_s^0 K^+ K^-$, or both.^{46,47,48} The idea is to fit the Dalitz-plot distribution of selected D^0 decays using the time-dependent formalism given in Eq. 23 (for D^0) and Eq. 24 (for \bar{D}^0). The variation of the decay amplitudes A_f , $A_{\bar{f}}$ and their conjugates across the Dalitz plot must be taken into account. We define $A(s_+, s_-)$ to be the amplitude for $D^0 \rightarrow K_s^0 h^+ h^-$ and $\bar{A}(s_+, s_-)$ to be the amplitude for $\bar{D}^0 \rightarrow K_s^0 h^+ h^-$, where s_+ and s_- are the coordinates of a given position in the Dalitz plot, e.g., $s_+, s_- \equiv m_{K_s^0 \pi^-}^2, m_{\pi^- \pi^+}^2$ (*CLEO*) or $s_+,$

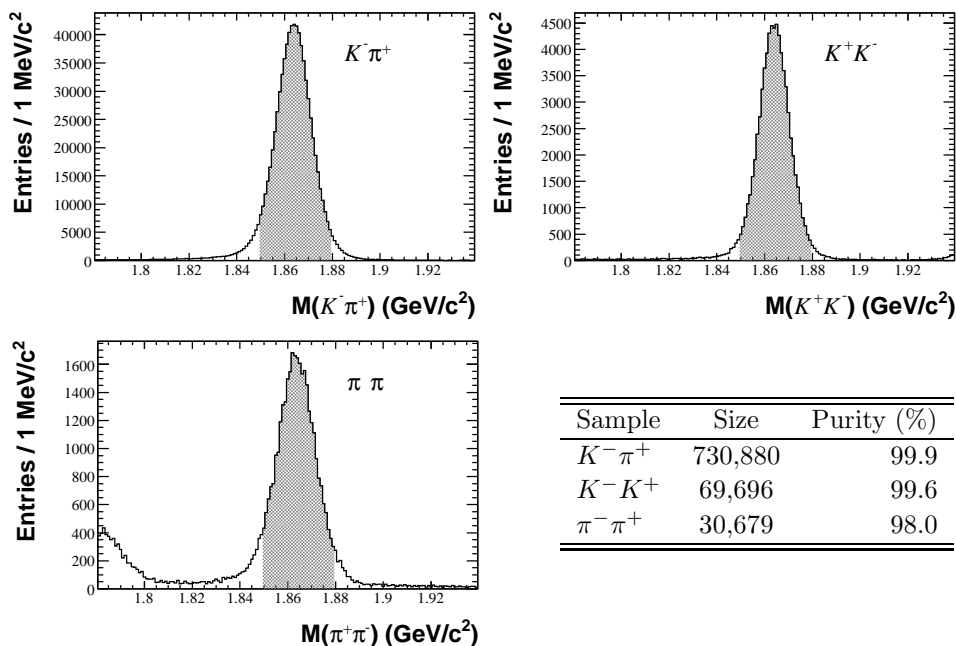


Fig. 10. The *BABAR* reconstructed D^0 mass distributions for the three D^0 tagged samples, within ± 0.8 MeV/ c^2 of the peak of Δm . The shaded region indicates the events used in the lifetime fit. (The structures appearing above 1.92 GeV/ c^2 in the $K^- K^+$ decay mode, and below 1.81 GeV/ c^2 in the $\pi^+ \pi^-$ decay mode, are mainly due to candidates with misidentified kaons or pions.) Also shown are the yield and purity of the three D^0 samples as calculated inside the ± 15 MeV/ c^2 mass window used in the lifetime measurements. Reprinted figure with permission from B. Aubert *et al.*, *Phys. Rev. D* 78, 011105(R) (2008). Copyright 2008 by the American Physical Society.⁴⁴

$s_- \equiv m_{K_s^0 \pi^+}^2, m_{K_s^0 \pi^-}^2$ (Belle, *BABAR*). In order to fit the Dalitz-plot distribution as a function of time, it is necessary to assume a Dalitz fit model. These models typically include a coherent sum of ten to twelve quasi-two-body intermediate resonances plus a non-resonant component. P - and D -wave amplitudes are modeled by Breit-Wigner or Gounaris-Sakurai functional forms, including Blatt-Weisskopf centrifugal barrier factors. In the *BABAR* analysis, the S -wave dynamics are modeled using a K -matrix formalism ($\pi\pi$), a Breit-Wigner plus non-resonant contribution ($K\pi$), and a coupled-channel Breit-Wigner model describing the $a_0(980)$ and Breit-Wigner models for the $f_0(1370)$ and $a_0(1450)$ (KK).

As far as mixing is concerned, the interesting Dalitz plot regions are where the CF and DCS amplitudes interfere and regions where CP eigenstates predominate.

These analyses proceed in a manner similar to the two-body, time-dependent analyses: they make use of the sign of the slow pion π_s from a D^{*+} decay to tag the neutral meson as D^0 or \bar{D}^0 at its creation. After selecting appropriate-quality charged tracks, $\pi^+ \pi^-$ pairs that have an invariant mass close to the K_s^0 mass (typically within 10 MeV) are selected, forming a K_s^0 candidate. Another set

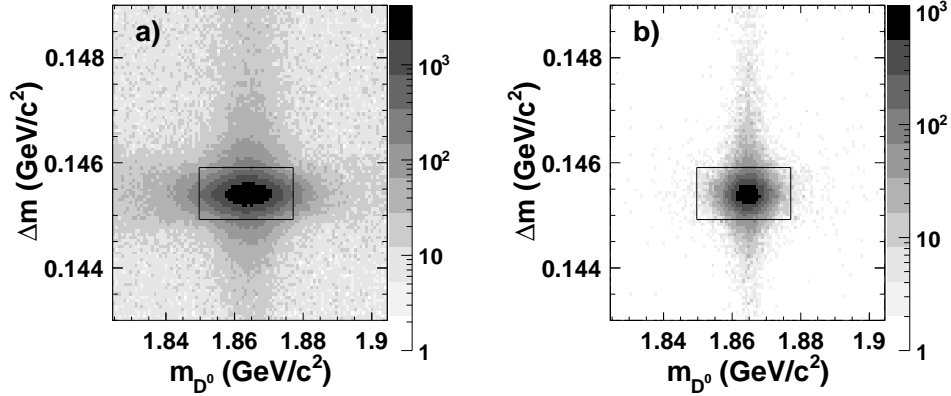


Fig. 11. BABAR distributions of m_{D^0} and Δm for the $K_S^0 h^+ h^-$ analysis, after all selection cuts. The shaded scale indicates the number density of events. The boxes indicate the signal regions as used in the analysis for the mixing fits. (a) $K_S^0 \pi\pi$. (b) $K_S^0 K^+ K^-$. Reprinted figures with permission from P. del Amo Sanchez *et al.*, *Phys. Rev. Lett.* 105, 081803 (2010). Copyright 2010 by the American Physical Society.⁴⁶

of oppositely-charged tracks that share a common vertex are combined with the K_S^0 candidate to form a D^0 candidate. This allows for the K_S^0 decay vertex to be displaced from the D^0 decay vertex. A kinematic fit then provides the D^0 decay position and its momentum vector p_{D^0} , which is required to point back the the luminous interaction region. The decay time t is calculated using the D^0 decay length $l = \beta\gamma ct = ctp_{D^0}/m_{D^0}$, along with its error σ_t , on an event-by-event basis.

Background sources include the random π_s background, where an incorrect assignment between a low-momentum pion and a good D^0 decay has been made, misreconstructed D^0 , and combinatoric background. A few other sources of backgrounds (classification varies from experiment to experiment) may also be included in the fit model as well to model specific non-signal decay modes.

The time-dependent analysis uses candidates from a two-dimensional signal region of $M_{D^0}^0$, the reconstructed D^0 candidate mass, and either Δm (BABAR), or $Q = m_{K_S^0 \pi \pi \pi_s} - m_{K_S^0 \pi \pi} - m_\pi$, the available kinetic energy released in the D^{*+} decay (Belle). See Fig. 11. BABAR (Belle) determines the yields of signal and background in the signal box by fitting the m_{D^0} and Δm (Q) to PDFs characterizing each background source over the full range in m_{D^0} and Δm (BABAR) or Q (Belle), and rescaling the component yields to the signal region. Belle finds 534,410 signal candidates in 540 fb^{-1} .⁴⁸ BABAR finds a signal yield of 540,800 (79,900) $K_S^0 \pi\pi$ ($K_S^0 K^+ K^-$) with purity 98.5% (99.2%) $K_S^0 \pi\pi$ ($K_S^0 K^+ K^-$) in 468.5 fb^{-1} of data.⁴⁶ Fig. 12 shows the Belle experiment's time-integrated distribution of D^0 decays and projections of the fit to the data where $m_\pm^2 = m_{K_S^0 \pi^\pm}^2$ for D^0 decays

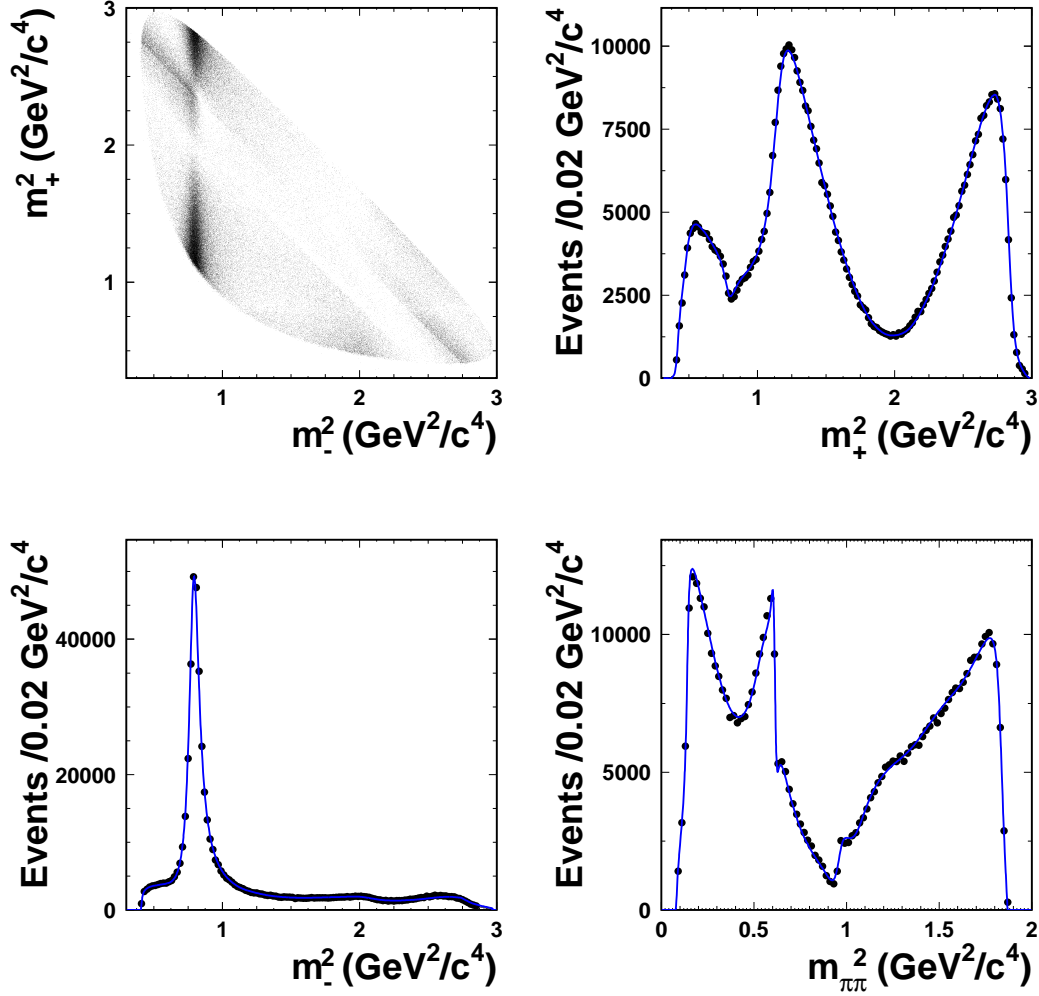


Fig. 12. Dalitz plot and fit projections for the Belle $D^0 \rightarrow K_S^0 \pi^+ \pi^-$ analysis. In the projections, the data are shown as points and the fit as a solid line. $m_{\pm}^2 = m_{K_S^0 \pi^{\pm}}^2$ for D^0 decays, and $m_{\pm}^2 = m_{K_S^0 \pi^{\mp}}^2$ for \bar{D}^0 decays. See Ref. 48 for details of the 18 quasi-two-body resonance plus non-resonant background Dalitz model and resulting fit. Reprinted figure with permission from L. M. Zhang *et al.*, *Phys. Rev. Lett.* 99, 131803 (2007). Copyright 2007 by the American Physical Society.

and $m_{\pm}^2 = m_{K_S^0 \pi^{\mp}}^2$ for \bar{D}^0 decays⁴⁸.

To determine the mixing parameters, PDFs are defined that include the dependence of the signal and background components on decay time t , σ_t , and location

in the Dalitz plot. Included in the signal PDF are the matrix elements

$$\mathcal{M}(s_-, s_+, t) = \mathcal{A}(s_-, s_+)g_+(t) + \frac{q}{p}\bar{\mathcal{A}}(s_-, s_+)g_-(t), \quad (63)$$

$$\bar{\mathcal{M}}(s_-, s_+, t) = \bar{\mathcal{A}}(s_-, s_+)g_+(t) + \frac{p}{q}\mathcal{A}(s_-, s_+)g_-(t), \quad (64)$$

which are convolved with a decay-time resolution function that depends on position in the Dalitz plot. Eqs. 63 and 64 are generalizations of Eqs. 17 and 18 to multi-body decays. Different resolution functions are used for $K_S^0\pi\pi$ and K_S^0KK distributions. The decay-time resolution function is a sum of Gaussians with widths that may scale with the event-by-event, decay-time error δt , and also depends weakly on position in the Dalitz plot. Belle uses three Gaussians with different scale factors and a common mean, which are allowed to vary in the fit. BABAR uses two Gaussians that scale with δt , one of which is allowed to have a non-zero mean (t_0 offset), and a third Gaussian which does not scale with δt . The results of this procedure are discussed in section 3.3.1.

2.3.2. $D^0 \rightarrow K^+\pi^-\pi^0$ Analysis

As in the case of the two-body WS decay $D^0 \rightarrow K^+\pi^-$, the three-body WS decay $D^0 \rightarrow K^+\pi^-\pi^0$ can occur through DCS decay or via $D^0 \rightarrow \bar{D}^0$ mixing followed by the CF decay $\bar{D}^0 \rightarrow K^+\pi^-\pi^0$. With a WS branching fraction of $(3.04 \pm 0.17) \times 10^{-4}$ compared with $(1.47 \pm 0.07) \times 10^{-4}$ for $D^0 \rightarrow K^-\pi^+$,¹⁹ the $K\pi\pi^0$ channel is competitive in sensitivity to the two-body channel, despite the lower efficiency of reconstructing the three-body final state.

Reconstruction details of $D^0 \rightarrow K\pi\pi^0$ events vary from experiment to experiment, but the basic selection process is as follows. The decay $D^{*+} \rightarrow \pi_s D^0$ is used to tag the flavor of the neutral D at production. To form D^0 candidates, pairs of oppositely charged tracks originating from a common vertex are combined with a π^0 candidate whose momentum in the laboratory is $\gtrsim 300$ MeV/c. D^0 candidates whose mass is within ~ 60 MeV/c² of the nominal D^0 mass are retained. Particle identification requirements are imposed to reduce feedthrough of doubly misidentified, CF candidates into the WS sample. The momentum of each D^0 candidate is required to point back to the interaction region and its momentum in the CM system (p^*) is required to satisfy $p^* \gtrsim 2.5$ GeV/c to suppress D^0 candidates from B decay.

Each D^0 candidate is paired with a slow pion π_s to form a D^{*+} candidate. D^{*+} candidates which have an appropriate value of Δm (or, equivalently, Q ; see Section 2.3.1) and have sufficiently good χ^2 per degree of freedom from the kinematic and/or vertex fits are retained.

Background sources considered are random π_s (an incorrectly associated π_s combined with good D^0 forming a D^{*+} candidate), incorrectly reconstructed charm decays, and uds combinatorial background. Maximum likelihood fits to the two-dimensional $(m_{K\pi\pi^0}, \Delta m)$ distribution are performed to determine the yields of

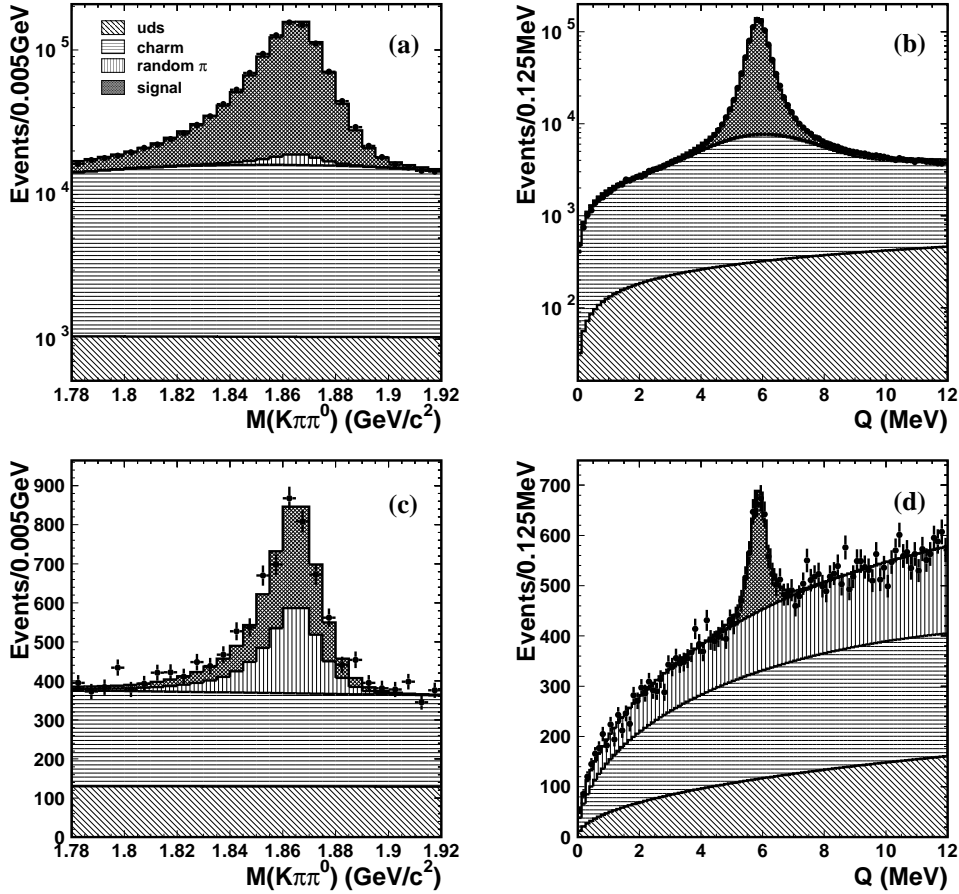


Fig. 13. Belle $K\pi\pi^0$ reconstructed mass ($m_{K\pi\pi^0}$) and available kinetic energy (Q) distributions, showing signal and background components as determined by a fit to the two-dimensional ($m_{K\pi\pi^0}$, Q) distribution. Top row: RS; bottom row: WS. Reprinted figure with permission from X.C. Tian *et al.*, *Phys. Rev. Lett.* 95, 231801 (2005). Copyright 2005 by the American Physical Society.⁴⁹

signal and background candidates in the RS and WS samples. As an example, see Fig. 13 for the Belle fit to the D^0 candidate mass and Q distributions.

BABAR analyzed the $D^0 \rightarrow K\pi\pi^0$ mode using two different methods. The first, method I,⁵⁰ uses the different decay-time dependence of DCS and mixed decays and analyzes regions of phase space chosen to optimize sensitivity to mixing. Although the rates of DCS and CF decays vary across the Dalitz plot, the mixing rate is the same at all phase space points.

The time dependence of the WS-to-RS decay rate ratio can be expressed for a given phase-space region (a tilde indicates integration of a quantity over this region)

as

$$\frac{\Gamma_{WS}^{K\pi\pi^0}(t)}{\Gamma_{RS}^{K\pi\pi^0}(t)} = \tilde{R}_D^{K\pi\pi^0} + \alpha \tilde{y}' \sqrt{\tilde{R}_D^{K\pi\pi^0}}(\Gamma t) + \frac{\tilde{x}'^2 + \tilde{y}'^2}{4}(\Gamma t)^2, \quad (65)$$

where α is an averaging factor that accounts for the variation of the strong phase over the phase space region ($0 \leq \alpha \leq 1$). \tilde{R}_D is the DCS branching ratio, \tilde{x}' and \tilde{y}' are the mixing parameters x and y rotated by an integrated strong phase $\tilde{\delta}$:

$$\begin{aligned} \tilde{x}' &= x \cos \tilde{\delta} + y \sin \tilde{\delta}, \\ \tilde{y}' &= -x \sin \tilde{\delta} + y \cos \tilde{\delta}. \end{aligned} \quad (66)$$

Note that $R_M = (\tilde{x}'^2 + \tilde{y}'^2)/2 = (x^2 + y^2)/2$ is independent of the integration region.

After signal and background yields are determined, a fit is performed to the decay-time distribution. The functional forms of the PDFs are determined based on MC studies, but all parameters are determined by fitting the data. The large RS signal is used to determine the resolution function used in the WS fit. The observed decay-time dependence of the WS PDF is given by Eq. 65 convolved with the resolution function. Projections of the reconstructed D^0 mass, Δm , and decay-time fits are shown in Fig. 14.

The second method (method II) used by *BABAR*⁵³ to search for mixing in $D^0 \rightarrow K\pi\pi^0$ decays is a time-dependent, Dalitz-plot analysis that uses an isobar model⁵⁴ to describe the dynamics. The time-dependent decay rate for WS decays to a particular final state f at a given point in the Dalitz plot $(s_{12}, s_{13}) = (m_{K^+\pi^-}^2, m_{K^+\pi^0}^2)$, and assuming $|x|, |y| \ll 1$, may be written as

$$\begin{aligned} \frac{dN_f(s_{12}, s_{13}, t)}{ds_{12}ds_{13}dt} = \\ e^{-\Gamma t} \left[|A_f|^2 + |A_f| |\bar{A}_f| (y \cos \delta_f - x \sin \delta_f) \Gamma t + \frac{x^2 + y^2}{4} |\bar{A}_f|^2 (\Gamma t)^2 \right], \end{aligned} \quad (67)$$

where $f = K^+\pi^-\pi^0$, the DCS amplitude is $A_f(s_{12}, s_{13}) = \langle f | \mathcal{H} | D^0 \rangle$, the CF amplitude is $\bar{A}_f(s_{12}, s_{13}) = \langle f | \mathcal{H} | \bar{D}^0 \rangle$, and $\delta_f(s_{12}, s_{13}) = \arg(A_f^* / \bar{A}_f)$.

Written in terms of normalized mixing parameters and normalized amplitude distributions, the time dependence can be expressed as:

$$\begin{aligned} \frac{dN_f(s_{12}, s_{13}, t)}{ds_{12}ds_{13}dt} \propto \\ e^{-\Gamma t} r_0^2 \left[|A_f^{\text{DCS}}|^2 + |A_f^{\text{DCS}}| |A_f^{\text{CF}}| (\hat{y} \cos \delta_f - \hat{x} \sin \delta_f) \Gamma t + \frac{\hat{x}^2 + \hat{y}^2}{4} |A_f^{\text{CF}}|^2 (\Gamma t)^2 \right], \end{aligned} \quad (68)$$

where $A_f^{\text{DCS}} = A_f / \sqrt{\int |A_f|^2 ds_{12} ds_{13}}$, $A_f^{\text{CF}} = \bar{A}_f / \sqrt{\int |\bar{A}_f|^2 ds_{12} ds_{13}}$ are normalized distributions, $r_0 = \sqrt{\int |A_f|^2 ds_{12} ds_{13} / \int |\bar{A}_f|^2 ds_{12} ds_{13}}$, and $\hat{x} = x/r_0$ and $\hat{y} = y/r_0$ are normalized mixing parameters.

The isobar model parametrizes the amplitudes A_f and \bar{A}_f as a coherent sum of seven resonances plus a $K\pi$ S -wave component derived from $K\pi$ scattering data,⁵⁵ including a non-resonant component. The high-statistics RS sample ($\sim 659,000$

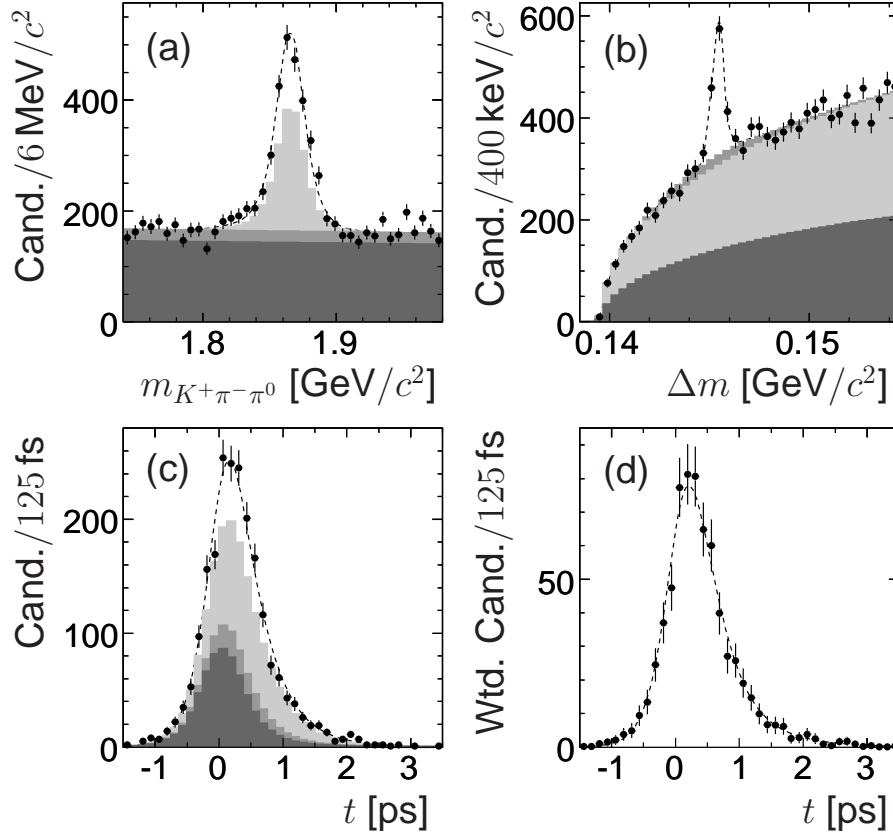


Fig. 14. BABAR fit projections for $K\pi\pi^0$ analysis method I (see text), showing data (points with error bars) and PDFs (dotted lines). (a) Reconstructed $m_{K\pi\pi^0}$ for candidates satisfying $0.1444 < \Delta m < 0.1464$ GeV/c^2 ; (b) Δm for candidates satisfying $1.85 < m_{K\pi\pi^0} < 1.88$ GeV/c^2 ; (c) decay-time t satisfying both mass selections in (a) and (b); and (d) signal-enhanced version of (c) using a channel-likelihood signal projection.^{51,52} Reprinted figure with permission from B. Aubert *et al.*, *Phys. Rev. Lett.* 97, 221803 (2006). Copyright 2006 by the American Physical Society.⁵⁰

candidates) is used to determine the isobar model parameters for CF decays and the decay-time resolution function for both the RS sample and the WS sample (~ 3000 candidates). See Fig. 15. Sensitivity to the mixing parameters arises primarily from the interference terms (linear in t) in Eq. 67 and Eq. 68. PDFs expressing the dependence of the WS decay rate on Dalitz plot position and decay time are convolved with the decay-time resolution and a fit performed, determining the DCS isobar model parameters (amplitudes and phases) and the mixing parameters.

An unknown strong phase difference $\delta_{K\pi\pi^0}$ between the DCS decay $D^0 \rightarrow \rho^- K^+$

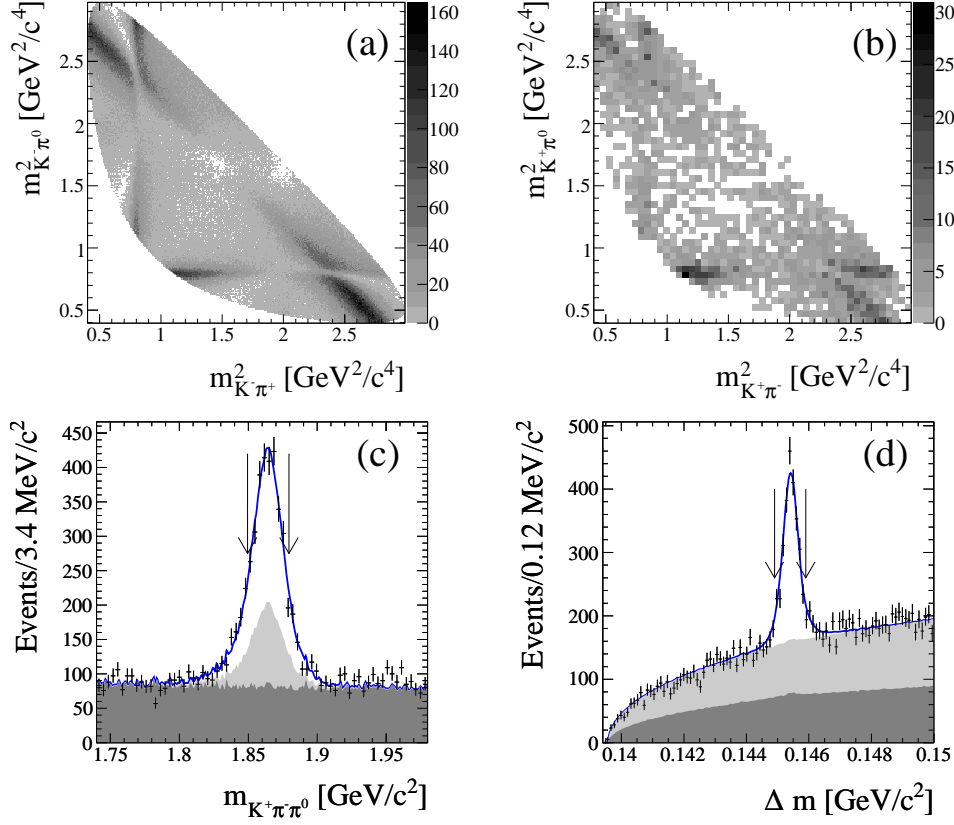


Fig. 15. BABAR RS (top left) and WS (top right) Dalitz distributions and reconstructed WS D^0 mass (bottom left) and Δm (bottom right) distributions for $D^0 \rightarrow K\pi\pi^0$ using method II. Shaded regions indicate signal (white), mistag background (gray), and combinatoric background (dark gray). Reprinted figure with permission from B. Aubert *et al.*, *Phys. Rev. Lett.* 103, 211801 (2009). Copyright 2009 by the American Physical Society.⁵³

and the CF decay $\bar{D}^0 \rightarrow K^+\rho^-$ cannot be determined in this analysis, so the mixing parameters measured are

$$\begin{aligned} x'_{K\pi\pi^0} &= x \cos \delta_{K\pi\pi^0} + y \sin \delta_{K\pi\pi^0}, \\ y'_{K\pi\pi^0} &= -x \sin \delta_{K\pi\pi^0} + y \cos \delta_{K\pi\pi^0}. \end{aligned} \quad (69)$$

Results of the two methods are discussed in Section 3.3.2.

2.3.3. $D^0 \rightarrow K^+\pi^-\pi^+\pi^-$ Analysis

The $D^0 \rightarrow K^-\pi^+\pi^-\pi^+$ (CF $K3\pi$) decay has been used to study charm physics since soon after the discovery of the D^+ and D^0 mesons. An early search for wrong-sign D^0 decays saw no significant signal, but did set limits on the WS rate.⁵⁶ E791

reported⁵⁷ a measurement attributed to DCS decay of $R_D^{K3\pi} = [0.25_{-0.34}^{+0.36} \pm 0.03]\%$ by analyzing the distribution of wrong-sign D^0 decay times. In a time-integrated measurement, CLEO reported evidence⁵⁸ for wrong-sign $D^0 \rightarrow K^+\pi^-\pi^+\pi^-$ decays. They found a 3.9 standard deviation result in the wrong-sign to right-sign branching fraction: $R_{WS}^{K3\pi} = [0.41_{-0.11}^{+0.12}(\text{stat}) \pm 0.04(\text{syst}) \pm 0.10(\text{phase space})]\%$.

The $D^0 \rightarrow K3\pi$ decay offers some advantages over $D^0 \rightarrow K\pi$, and a couple of difficulties. One advantage is that the RS branching fraction for $D^0 \rightarrow K\pi\pi\pi$ of $\approx 8.1\%$ is twice that of $D^0 \rightarrow K\pi$ of $\approx 3.9\%$. Another is that the vertex resolution of the four-body $K3\pi$ decay is usually better than that of the two-body $K\pi$ decay, which leads to an improved decay-time resolution. These advantages are somewhat offset by the reduced efficiency of reconstructing the four-body decay relative to the two-body decay and by complications in determining the mixing parameters x and y due to variations in the strong phase over the four-body phase space (the mixing rate R_M , however, is independent of position in phase space). As in the case of $D^0 \rightarrow K\pi\pi^0$, the strong phase $\delta_{K\pi\pi\pi}$ cannot be determined in this analysis alone. To date, no amplitude analysis of $D^0 \rightarrow K3\pi$ decays has been attempted.

2.3.4. Analysis of Wrong-sign Semileptonic Decays

The WS semileptonic decays $D^0 \rightarrow K^{(*)+}e^-\bar{\nu}_e$ and $D^0 \rightarrow K^{(*)+}\mu^-\bar{\nu}_\mu$ offer unique features to searches for D^0 - \bar{D}^0 mixing. One unique feature is that doubly Cabibbo-suppressed, wrong-sign decays do not occur in the semileptonic mode in the SM. This simplifies the time-dependence of the WS rate relative to the RS rate, Eq. 59, to:

$$R_{WS}(t) = \frac{R_M}{2}(\Gamma t)^2. \quad (70)$$

The WS decay rate is thus directly sensitive to the presence of mixing, as there is no contribution from either DCS decay or from interference between DCS decay and mixing. On the other hand, semileptonic decays present a challenge not encountered when analyzing hadronic decays: the presence of the unobserved neutrino in the final state precludes exact determination of the D^0 candidate mass, leading to degraded decay-time and mass-difference resolutions and higher backgrounds.

Distinguishing characteristics of mixing in WS semileptonic decays include the quadratic time dependence of Eq. 70 and a peak in the available kinetic energy spectrum $Q = m(Kl\nu\pi_s) - m(D^0) - m(\pi)$ near 5.8 MeV/ c^2 (or, equivalently, in $\Delta m = m(Kl\nu\pi_s) - m(Kl\nu)$ near 145 MeV/ c^2). WS semileptonic decays share the peaking behavior in Q (or Δm) with RS semileptonic decays, but have a time dependence modified by the quadratic term given in Eq. 70 instead of the pure exponential decay-time distribution characterizing the RS decay. Semileptonic decays are also susceptible to feed-through from RS $D^0 \rightarrow K\pi$ decays, where the kaon is mis-identified as a lepton and the pion as a kaon. This is particularly a concern in the case of semi-muonic decays, since the kaons and pions are more prone to mis-identification as muons than as electrons.

Many searches for mixing using semileptonic decays have been carried out. The $K\mu\nu$ mode in particular has been used to search for and set limits on mixing since shortly after the discovery of the D^0 meson.^{59,60} More recently, E791, CLEO, Belle, and *BABAR* have reported measurements.^{61,62,63,64,65}

The E791 analysis estimates the missing momentum of the neutrino by using the measured decay vertex positions of the D^{*+} and the D^0 , the kaon and lepton momenta, and attributing the D^0 mass to the secondary decay. This results in a two-fold ambiguity, which is resolved by always choosing the higher-momentum solution for the D^0 (motivated by MC studies). This choice results in some degradation in the decay-time resolution which is accounted for as a systematic error.

The Belle analysis applies the following procedure to estimate the neutrino four-momentum and consequently, Δm . Applying four momentum balance to the initial e^+e^- system, the Kl system, the missing ν , and the rest of the event, an approximation for the missing momentum is obtained. This value is refined by the use of two additional constraints. First, a D^0 mass constraint is applied to the $Kl\nu$ system, resulting in a scale factor that is used to produce a refined $m(Kl\nu\pi_s)$ value, the $m(Kl\nu)$ mass having been fixed to $m(D^0)$. A second constraint on m_ν^2 is applied, resulting in a correction to the angle between the three-momentum of the Kl system and that of the rest of the event.

BABAR has published two semileptonic mixing analyses, one using a single-tag ($D^{*+} \rightarrow D^0\pi_s^+$) method and the other using a double-tag method. The single-tag analysis includes both $D^0 \rightarrow K e \nu$ and $D^0 \rightarrow K^* e \nu$ decays, and treats them essentially the same way. No attempt is made to reconstruct the K^* explicitly; its kaon daughter is used directly in reconstructing the D^0 , as if it were a D^0 daughter. After selection cuts are imposed, resulting K , e , and π_s tracks, the position of the K - e vertex, and the event thrust axis are used to reconstruct the three components of the D^0 momentum vector by means of three neural net estimators. These estimators have been trained using $\mathcal{O}(10^5)$ simulated signal events to reproduce the D^0 momentum vector components. Events are required to pass a neural net selection which discriminates prompt charm from background events. The majority of the remaining background comes from charm events not from B decays where a random charged pion has been combined with a charged K daughter and an electron daughter from the charm decay, or with K and electron combinations not from a common parent. Understanding the origin of these backgrounds is important as they do not share exactly the same decay-time distribution as true charm decays, and this must be accommodated in the decay-time fit. After performing an extended maximum likelihood fit to the large RS data sample, which determines many of the PDF parameters describing the RS and WS Δm and decay-time PDFs, the mixing quantities are determined from a fit to the WS data, including the decay-time information.

The *BABAR* double-tagged analysis attempts to address the predominant background present in the singly-tagged analysis: feedthrough into the WS sample from RS semileptonic D^0 decays, where the D^0 has been wrongly associated with a ran-

dom slow pion π_s . In addition to the D^{*+} tag, a second tag is constructed by requiring either a fully reconstructed, high-momentum, hadronically decaying D^0 or D^+ in the the opposite hemisphere. While greatly improving the purity of the tagged sample, the selection efficiency drops by more than a factor of ten. Additional background suppression criteria are imposed which bring the sensitivity of this analysis to about the same as the single-tag analysis above. Resulting Δm distributions for RS and WS events are shown in Fig. 16.

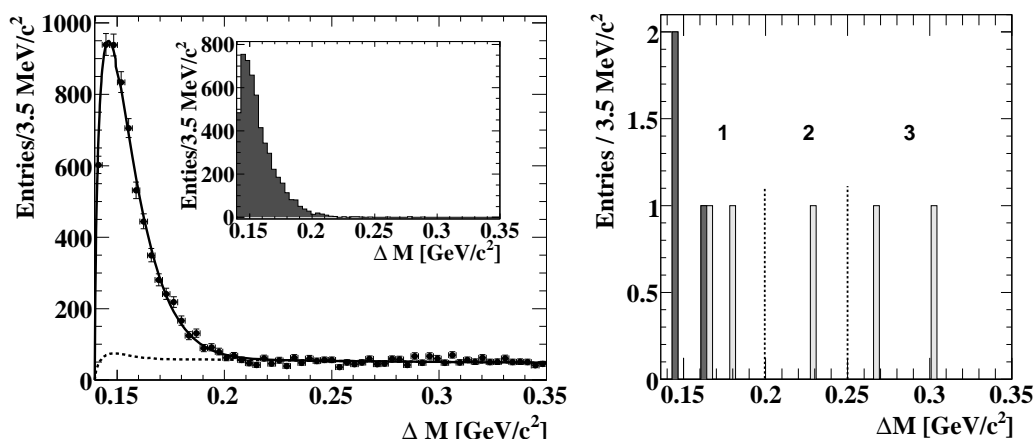


Fig. 16. BABAR semileptonic Δm distributions from Ref. 64, showing both singly-tagged (white) and doubly-tagged distributions (gray) Left plot: RS data (points) before the double-tag selection, along with the total fit projection (solid line), and the background fit projection (dashed line). Inset: RS Δm distribution after applying the double-tag selection. Right plot: WS data events satisfying all selection criteria (gray histogram) and all but the double-tag selection (white histogram). Reprinted figures with permission from B. Aubert *et al.*, *Phys. Rev. D* 76, 014018 (2007). Copyright 2007 by the American Physical Society.

3. Current Experimental Results

3.1. Time-independent Experiments

3.1.1. Correlated decay results at 3.770 GeV

Using methods described in Section 2.1.1, the CLEO Collaboration reported the first measurement of the strong phase difference $\delta_{K\pi}$ in 2008.^{31,35} From 281 pb^{-1} of data collected at $\sqrt{s} = 3.770$ GeV with the CLEO-c detector, the correlated analysis was performed using different sets of external measurements as input. These included: measurements of two-body D^0 branching fractions; the previous, plus measurements of the time-integrated WS rate $R_{WS} \equiv \Gamma(D^0 \rightarrow K^+\pi^-)/\Gamma(D^0 \rightarrow K^-\pi^+)$ and the mixing rate R_M (the “standard” fit); and the previous, plus mea-

measurements of x , y , x'^2 , y' , and r^2 (the “extended” fit). Correlations between external inputs were incorporated in the fits. In the standard fit, $x \sin \delta_{K\pi}$ is fixed to zero. In the extended fit, this condition is relaxed.

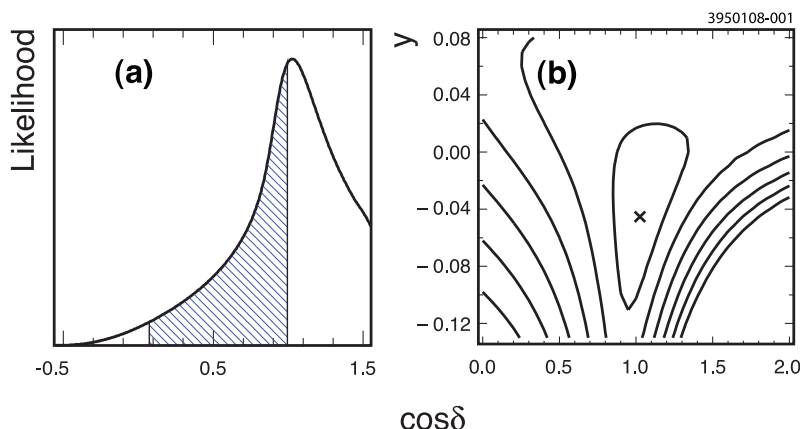


Fig. 17. Fit likelihood from the CLEO standard fit, including statistical and systematic uncertainties. (a) For $\cos \delta$; the hatched region contains 95% of the physically allowed area. (b) Two-dimensional likelihood for $\cos \delta$ and y . Reprinted figure with permission from J. Rosner *et al.*, *Phys. Rev. Lett.* 100, 211801 (2008). Copyright 2008 by the American Physical Society.³¹

Systematic uncertainties accounted for in the analyses included estimates of efficiencies for particle identification, reconstructing tracks, and for reconstructing neutral neutral decays (K_S^0 and π^0). Other systematic uncertainties included efficiencies for η reconstruction, selection cuts, fit model description, and detector and physics modeling. The largest systematics were for η reconstruction (4.0%) and $\Delta E = E_{D^0} - E_{\text{beam}}$ selection (0.5–5.0%). Bias estimates on the fitting procedure were obtained by studying a sample of simulated $D^0\bar{D}^0$ decays fifteen times the size of the recorded dataset. Biases from the fitting procedure were less than one-half the size of the statistical errors on the fitted parameters.

Results from the standard and extended fits are given in Table 2. Likelihoods from the standard fit are shown in Fig. 17 and from the extended fit are shown in Fig. 18. The final result for $\delta_{K\pi}$, including asymmetric errors estimated from the shape of the likelihood function shown in Fig. 17, is $\cos \delta_{K\pi} = 1.03^{+0.31}_{-0.17} \pm 0.06$. Limiting to the region $|\cos \delta_{K\pi}| < 1$, $|\delta_{K\pi}| < 75^\circ$ at the 95% confidence level. From the extended fit, they obtain $\cos \delta_{K\pi} = 1.10 \pm 0.35 \pm 0.07$ and $x \sin \delta_{K\pi} = (4.4^{+2.7}_{-1.8} \pm 2.9) \times 10^{-3}$ and $\delta_{K\pi} = (22^{+11+9}_{-12-11})^\circ$. In both cases, the statistical errors were obtained by inspection of the log likelihood.

In a recent preliminary analysis,³² CLEO extended its quantum correlated coherent decay analysis to measure the strong phase differences in $D^0 \rightarrow K^+\pi^-$,

Table 2. CLEO mixing and $\delta_{K\pi}$ strong phase difference measurements. From Refs. 31 and 35. See text for fit descriptions.

Parameter	Standard fit	Extended fit
y	$(-45 \pm 59 \pm 15) \times 10^{-3}$	$(6.5 \pm 0.2 \pm 2.1) \times 10^{-3}$
x^2	$(-1.5 \pm 3.6 \pm 4.2) \times 10^{-3}$	$(0.06 \pm 0.01 \pm 0.05) \times 10^{-3}$
r^2	$(8.0 \pm 6.8 \pm 1.9) \times 10^{-3}$	$(3.44 \pm 0.01 \pm 0.09) \times 10^{-3}$
$\cos \delta_{K\pi}$	$1.03^{+0.31}_{-0.17} \pm 0.06$	$1.10 \pm 0.35 \pm 0.07$
$x \sin \delta_{K\pi}$	Fixed at 0	$(4.4^{+2.7}_{-1.8} \pm 2.9) \times 10^{-3}$
$\delta_{K\pi}$	—	$(22^{+11+9}_{-12-11})^\circ$

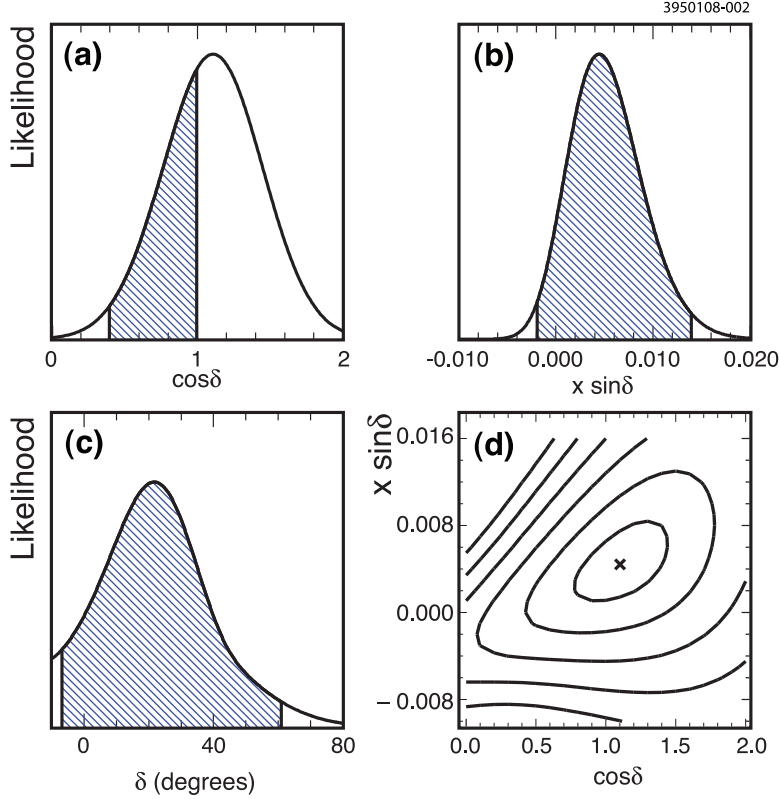


Fig. 18. Fit likelihoods from the CLEO extended fits, including statistical and systematic uncertainties. Hatched regions contain 95% of the physically allowed area. (a) $\cos \delta$. (b) $x \sin \delta$. (c) δ . (d) Two dimensional likelihood for $\cos \delta$ and $x \sin \delta$. Reprinted figure with permission from J. Rosner *et al.*, *Phys. Rev. Lett.* 100, 211801 (2008). Copyright 2008 by the American Physical Society.³¹

$D^0 \rightarrow K^+ \pi^- \pi^0$, $D^0 \rightarrow K^+ \pi^- \pi^+ \pi^-$ and $D^0 \rightarrow K_{S,L}^0 h^+ h^-$, $h = \pi, K$, using the full dataset (818 pb^{-1}) together with additional single- and double-tag modes. This

analysis makes direct measurements of $r_{K\pi}^2$ and $\sin \delta_{K\pi}$, resulting in approximately a factor of two smaller (and more symmetric) statistical uncertainties on $\cos \delta_{K\pi}$. In the near future, BES-III will likely produce strong phase difference measurements with improved statistical precision.

3.2. Results from Time-dependent Analyses of Two-body Decays

3.2.1. $D^0 \rightarrow K^+\pi^-$ Wrong-sign Decay Results

Several experiments, E691,⁶⁶ E791,⁵⁷ FOCUS,⁶⁷ CLEO,⁶⁸ BABAR,⁶⁹ and Belle⁷⁰ have set upper limits on $D^0\text{-}\bar{D}^0$ mixing by analyzing the time dependence of WS $D^0 \rightarrow K^+\pi^-$ decays outlined in Sec. 2.2.1. Of these, the Belle limit, based on 400 fb^{-1} , is the most stringent. Assuming CP conservation, they find: $x'^2 < 0.72 \times 10^{-3}$ and $-9.9 \times 10^{-3} < y' < 6.8 \times 10^{-3}$ at the 95% confidence level.

In 2007 the BABAR Collaboration reported evidence for $D^0\text{-}\bar{D}^0$ mixing from (4030 ± 90) WS signal candidates and (1141500 ± 1200) RS signal candidates in a 384 fb^{-1} data sample.¹² The reconstructed decay-time distribution for WS data and the fit results with and without mixing (assuming CP conservation) are shown in Fig. 19. The fit with mixing provides a substantially better description of the data than the fit with no mixing. The parameters obtained from fitting the BABAR data assuming CP conservation are listed in Table 3.

In the BABAR measurement, the significance of the mixing signal is estimated from the change in the log likelihood, $-2\Delta \log \mathcal{L}$, with respect to its value at the global minimum. Fig. 20 shows the confidence-level contours calculated using the change in log likelihood from the joint estimation of two parameters. The best fit value of the (x'^2, y') parameters to the BABAR data is at the unphysical value of $(x'^2 = -2.2 \times 10^{-4}, y' = 9.7 \times 10^{-3})$. As can be seen from Fig. 20, the two parameters are highly correlated with each other. Constraining the fit region to $x'^2 \geq 0$ yields $(x'^2 = 0, y' = 6.4 \times 10^{-3})$, and corresponds to $-2\Delta \log \mathcal{L} = 0.7$. The no-mix point corresponds to $-2\Delta \log \mathcal{L} = 23.9$ statistical units. The maximum log likelihood is denoted as $\log \mathcal{L}(x'^2, y')$. Each systematic variation is included one at a time into the fit and a new log likelihood $\log \mathcal{L}(x'^2_i, y'_i)$ is obtained. The significance of the i^{th} systematic variation is $s_i^2 = 2 \left[\log \mathcal{L}(x'^2, y') - \log \mathcal{L}(x'^2_i, y'_i) \right] / 2.3$, where the factor of 2.3 is the 68% confidence level for two degrees of freedom. Reducing $-2\Delta \log \mathcal{L}$ by $1 + \sum_i s_i^2 = 1.3$ everywhere to account for systematic uncertainties results in a significance equivalent to 3.9 standard deviations. Predominant systematic uncertainties on the mixing parameters arise from modeling the long decay times of other charm decays populating the signal region and to a non-zero mean in the proper decay-time resolution function.

To allow for CPV , the BABAR analysis fits the D^0 and \bar{D}^0 samples separately to determine the parameters (R_D^+, x'^{++}, y'^+) and $(R_D^-, x'^{- -}, y'^-)$, respectively. From these fitted values, the parameters $R_D = \sqrt{R_D^+ R_D^-}$ and $A_D = (R_D^+ - R_D^-) / (R_D^+ + R_D^-)$ are computed. The systematic component of the error on the BABAR measurement

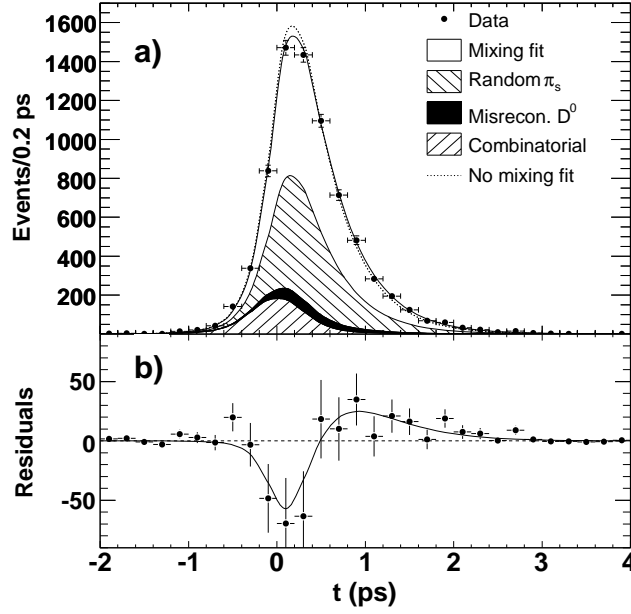


Fig. 19. BABAR: (a) Projections of the reconstructed decay-time distribution of D^0 and \bar{D}^0 WS candidates (points with error bars) and fit result integrated over the region $1.843 < m_{K\pi} < 1.883 \text{ GeV}/c^2$ and $0.1445 < \Delta m < 0.1465 \text{ GeV}/c^2$. Assuming CP conservation, the results of fitting with mixing and without mixing are shown as the solid and dashed curves, respectively. (b) The points with error bars represent the difference between the data and the average value of the no-mixing fit in each data bin. The solid curve shows the difference between the fit with and without mixing. If there were no mixing, the data points would scatter randomly around the dashed horizontal line. Reprinted figure with permission from B. Aubert *et al.*, *Phys. Rev. Lett.* 98, 211802 (2007). Copyright 2007 by the American Physical Society.¹²

of A_D is mainly due to uncertainties in modeling the slight asymmetry between the interactions of K^+ and K^- mesons in the detector.

The CDF Collaboration, using a 1.5 fb^{-1} data sample of $\bar{p}p$ collisions at $\sqrt{s} = 1.96 \text{ TeV}$ has shown evidence for mixing in the $D^0 \rightarrow K^+\pi^-$ channel.¹⁴ Since the CDF experiment was not running on the $\Upsilon(4S)$ as BABAR and Belle were, removal of $B \rightarrow D$ decays was considerably more challenging than applying a simple center of mass momentum cut, as was done in the B -factory measurements. On the other hand, due to the much larger average boost, the average flight distance in the lab is greater than in the B -factory experiments. Despite the vastly different environment, the central values of the mixing parameters shown in Table 3 and the (x'^2, y') C.L. contours shown in Fig. 21, both from the CDF experiment, agree remarkably well with the corresponding BABAR results. There is no evidence for CPV from any of the reported measurements.

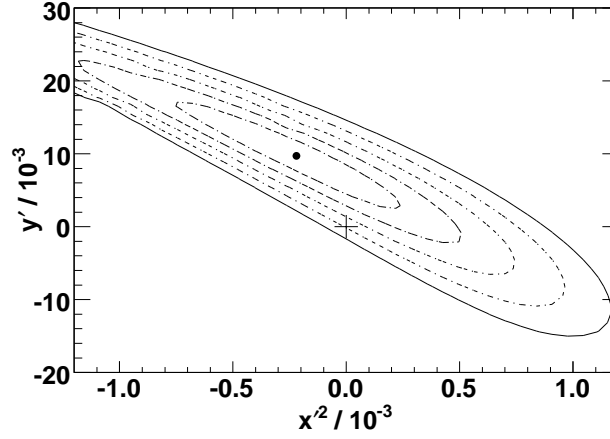


Fig. 20. *BABAR*: The best fit value for the mixing parameters (x'^2, y') (\bullet), the no-mix point $(0, 0)$ ($+$), and confidence level (C.L.) contours evaluated for $(1 - \text{C.L.}) = 0.317$ (1σ), 4.55×10^{-2} (2σ), 2.70×10^{-3} (3σ), 6.33×10^{-5} (4σ) and 5.73×10^{-7} (5σ), using the change $-2\Delta \log \mathcal{L}$ from the joint estimation of two parameters. The contours include the estimated systematic uncertainty. Reprinted figure with permission from B. Aubert *et al.*, *Phys. Rev. Lett.* 98, 211802 (2007). Copyright 2007 by the American Physical Society.¹²

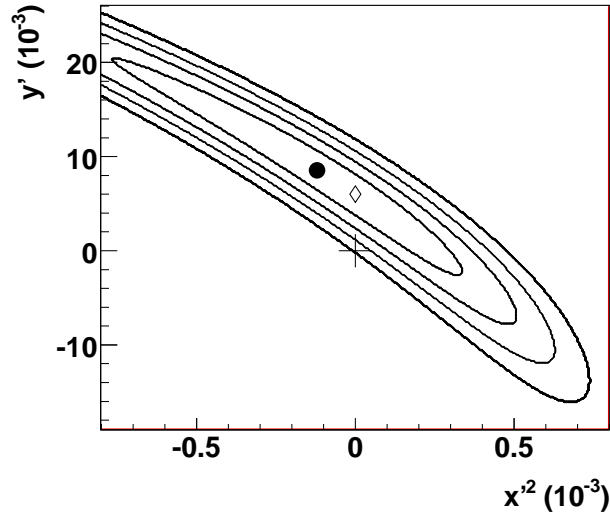


Fig. 21. *CDF*: The unconstrained best fit value for the mixing parameters (x'^2, y') (\bullet), requiring $(x'^2 \geq 0)$ (\diamond), the $(0, 0)$ (no-mix) point ($+$) and Bayesian probability contours corresponding to one through four equivalent Gaussian standard deviations. Reprinted figure with permission from T. Aaltonen *et al.*, *Phys. Rev. Lett.* 100, 121802 (2008). Copyright 2008 by the American Physical Society.¹⁴

Table 3. $D^0\bar{D}^0$ mixing and CPV parameters from $D^0 \rightarrow K^+\pi^-$ decays. For results with two reported uncertainty components, the first is statistical and the second is systematic. The results with a single uncertainty component include both statistical and systematic uncertainties.

Fit type	Parameter	Fit Results ($/10^{-3}$)		
		<i>BABAR</i> ¹²	CDF ¹⁴	Belle ⁷⁰
No CPV or mixing	R_D	$3.53 \pm 0.08 \pm 0.04$	4.15 ± 0.10	$3.77 \pm 0.08 \pm 0.05$
No CPV	R_D	$3.03 \pm 0.16 \pm 0.10$	3.04 ± 0.55	3.64 ± 0.17
	x'^2	$-0.22 \pm 0.30 \pm 0.21$	-0.12 ± 0.35	$0.18^{+0.21}_{-0.23}$
	y'	$9.7 \pm 4.4 \pm 3.1$	8.5 ± 7.6	$0.6^{+4.0}_{-3.9}$
Significance		3.9	3.8	2.0
CPV allowed	R_D	$3.03 \pm 0.16 \pm 0.10$	—	—
	A_D	$-21 \pm 52 \pm 15$	—	23 ± 47
	A_M	—	—	670 ± 1200
	x'^{++2}	$-0.24 \pm 0.43 \pm 0.30$	—	—
	y'^{+}	$9.8 \pm 6.4 \pm 4.5$	—	—
	x'^{-2}	$-0.20 \pm 0.41 \pm 0.29$	—	—
	y'^{-}	$9.6 \pm 6.1 \pm 4.3$	—	—
	x'^2	—	—	< 0.72 (95% C.L.)
	y'	—	—	$-28 < y' < 21$ (95% C.L.)

3.2.2. D^0 Lifetime Ratio Results

E791, FOCUS, CLEO, Belle, and *BABAR* have published y_{CP} results^{13,42,44,45,72,73} from lifetime measurements of $D^0 \rightarrow K^+K^-$ and $D^0 \rightarrow \pi^+\pi^-$ decays relative to that from $D^0 \rightarrow K^-\pi^+$ decays. Fits to the proper time distributions from the *BABAR* untagged analysis⁴⁵ are shown in Fig. 22. The lifetime measurement is determined from a fit using the decay time and decay-time error of candidates in a signal region, as described in Sec. 2.2.2. The charm background component shape and yield in the signal region are obtained from MC simulated events. The combinatorial background component shape in the signal region is estimated from sideband data. A fit to the D^0 data mass distribution is performed over the full mass range to estimate the total background and signal yields in the signal region. The combinatorial yield in the signal region is then obtained by subtracting the charm background yield from the total background yield there.

The results from the Belle and *BABAR* experiments on A_Γ show no evidence for CP violation. These measurements are shown at the bottom of Table 4. Results for y_{CP} are shown in Fig. 23, and are given in Table 4. The Heavy Flavor Averaging Group (HFAG) world average y_{CP} value^{15,71} is more than four standard deviations away from the no-mixing hypothesis ($y_{CP} = 0$).

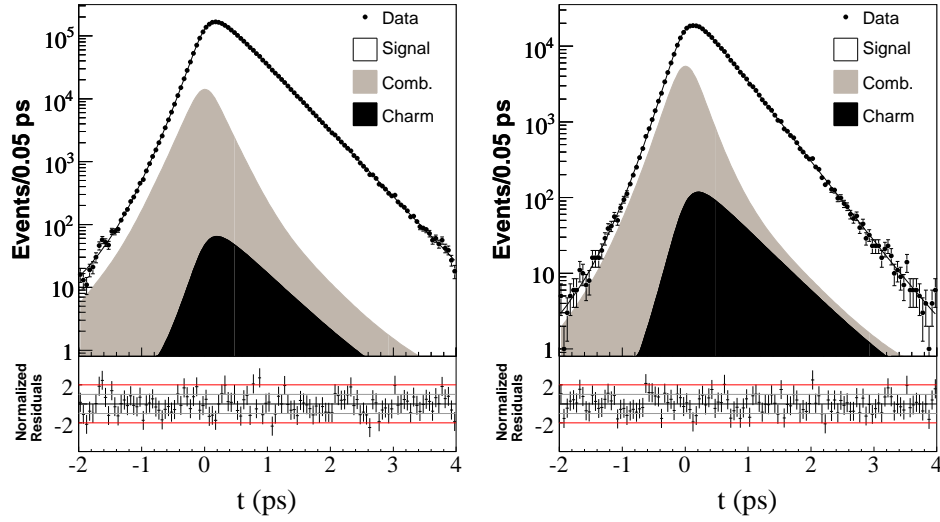


Fig. 22. BABAR decay-time distributions of $D^0 \rightarrow K^- \pi^+$ (left), and $D^0 \rightarrow K^+ K^-$ (right), from untagged D^0 decays. In each plot, the total fit is shown as a solid line. Fit components are signal (white), combinatorics (gray), and charm background (black). Reprinted figures with permission from B. Aubert *et al.*, *Phys. Rev. D* 80, 071103(R) (2009). Copyright 2009 by the American Physical Society.⁴⁵

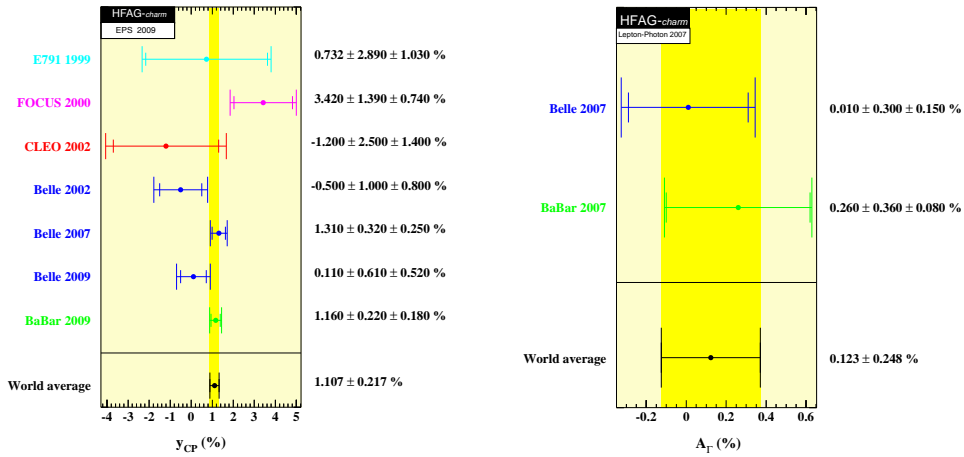


Fig. 23. HFAG compendium of y_{CP} (left) and A_Γ (right) measurements, along with world average values. From Refs. 15, 71.

Table 4. Results from y_{CP} ($\Delta\Gamma$) and A_Γ measurements from E791, FOCUS, CLEO, Belle, and BABAR experiments.^{13,42,44,45,72,73} Measurement uncertainties are given as statistical (first) and systematic (second). The world-average uncertainty is statistical and systematic combined.

Experiment	Parameter	Result (%)	data sample
E791 ⁴²	$\Delta\Gamma$	$0.04 \pm 0.14 \pm 0.05$	500 GeV πN interactions (2×10^{10} events)
FOCUS ⁷²	y_{CP}	$3.42 \pm 1.39 \pm 0.74$	γN interactions (1×10^6 reconstr. $D \rightarrow Kn(\pi)$)
CLEO ⁷³	y_{CP}	$1.2 \pm 2.5 \pm 1.4$	9.0 fb^{-1} near $\Upsilon(4S)$ resonance ; untagged
Belle ¹³	y_{CP}	$0.5 \pm 1.0^{+0.7}_{-0.8}$	23.4 fb^{-1} near $\Upsilon(4S)$ resonance; untagged
Belle ¹³	y_{CP}	$1.31 \pm 0.32 \pm 0.25$	540 fb^{-1} near $\Upsilon(4S)$ resonance ; D^* tagged
Belle ¹³	y_{CP}	$0.11 \pm 0.61 \pm 0.52$	673 fb^{-1} near $\Upsilon(4S)$ resonance ; $D \rightarrow (K^+ K) K^0$
BABAR ⁴⁴	y_{CP}	$1.03 \pm 0.33 \pm 0.19$	384 fb^{-1} near $\Upsilon(4S)$ resonance ; D^* tagged
BABAR ⁴⁵	y_{CP}	$1.12 \pm 0.26 \pm 0.22$	384 fb^{-1} near $\Upsilon(4S)$ resonance ; untagged
BABAR ⁴⁵	y_{CP}	$1.16 \pm 0.22 \pm 0.18$	D^* tagged + untagged combined
HFAG ⁷¹	y_{CP}	1.107 ± 0.217	World Average
Belle ¹³	A_Γ	$0.01 \pm 0.30 \pm 0.15$	540 fb^{-1} near $\Upsilon(4S)$ resonance ; D^* tagged
BABAR ⁴⁴	A_Γ	$0.26 \pm 0.36 \pm 0.08$	384 fb^{-1} near $\Upsilon(4S)$ resonance ; D^* tagged
HFAG ⁷¹	A_Γ	0.123 ± 0.248	World Average

3.3. Results from Time-dependent Analyses of Multi-body Decays

3.3.1. $D^0 \rightarrow K_s^0 h^+ h^-$ Analysis Results

CLEO⁴⁷, Belle^{48,74}, and BABAR⁴⁶ have published results from time-dependent Dalitz-plot analyses of $D^0 \rightarrow K_s^0 \pi^+ \pi^-$ decays and $D^0 \rightarrow K_s^0 K^+ K^-$ (Belle, BABAR). The CLEO Collaboration, which pioneered this technique, set 95% confidence level (CL) limits on the mixing parameters x and y . Results for x and y are given in Table 5 and world averages in Fig. 25. No evidence for CP violation has been seen by any of the experiments.

Experimental systematics include variations in background and PDF models, efficiencies, event selection criteria, and experimental resolution effects. In addition to these, systematics from the chosen resonance decay model are evaluated as well.

Additional cross-checks are performed. Fitted values of background fractions, D^0 lifetimes, and decay-time scale factors are determined to be consistent with expectations or previous results. Decay-time distributions are shown in Fig. 24. Belle, CLEO, and BABAR perform additional mixing fits to check for CP violation. BABAR performs separate fits to D^0 and \bar{D}^0 decays, and no evidence for CP violation in mixing is seen. CLEO performs separate fits to D^0 and \bar{D}^0 samples. Belle incorporates additional CP -violating parameters in their mixing fit. These additional fits yield results consistent with the nominal fitted values. No evidence for CP violation is seen in any of the measurements.

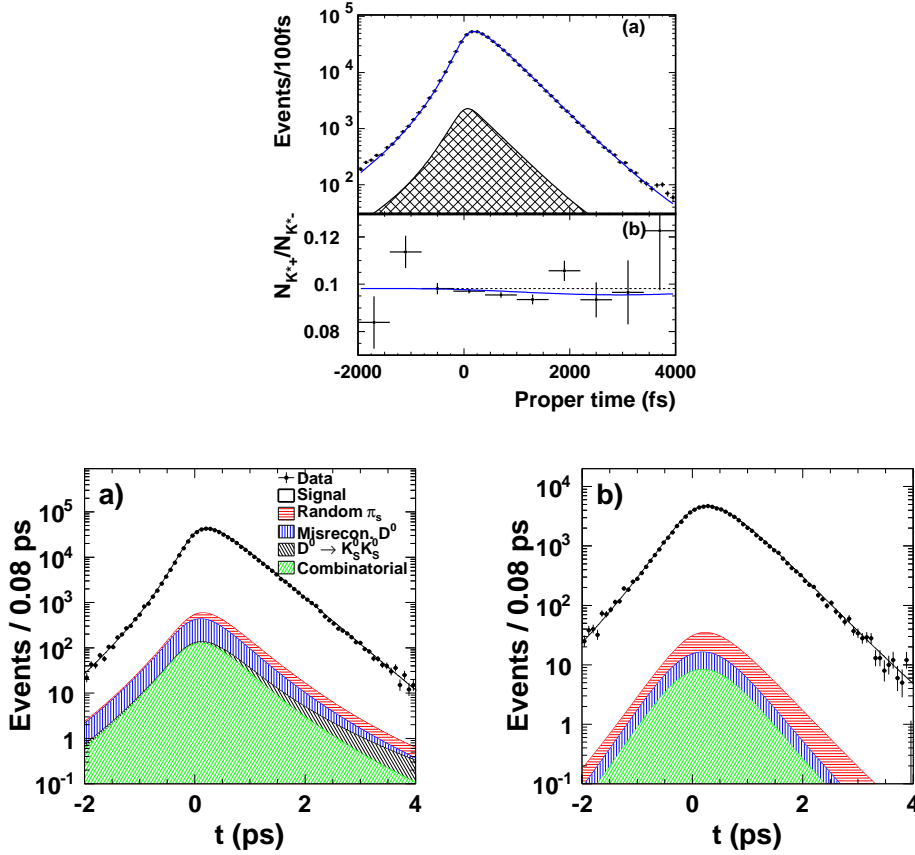


Fig. 24. Reconstructed $K_S^0 h^+ h^-$ decay-time distributions. Top: Belle $K_S^0 \pi^+ \pi^-$. Bottom left: BABAR, $K_S^0 \pi^+ \pi^-$. Bottom right: BABAR, $K_S^0 K^+ K^-$. Reprinted figures with permission from L.M. Zhang *et al.*, *Phys. Rev. Lett.* 99, 131803 (2007) and P. del Amo Sanchez *et al.*, *Phys. Rev. Lett.* 105, 081803 (2010) Copyright 2007 and 2010 by the American Physical Society.^{46,48}

3.3.2. $D^0 \rightarrow K \pi \pi^0$ Analysis Results

The first observation of the WS decay mode $D^0 \rightarrow K^+ \pi^- \pi^0$ was reported by CLEO in 2001.⁷⁵ Using a 9 fb^{-1} dataset of e^+e^- collisions near the $\Upsilon(4S)$ resonance, they observed the decay with a 4.9 standard deviation significance and reported a wrong-sign rate of $R_{WS}^{K\pi\pi^0} = [0.43^{+0.11}_{-0.10} \pm 0.07]\%$. Using 281 fb^{-1} of e^+e^- colliding-beam data near the $\Upsilon(4S)$, Belle (2005) reported⁴⁹ a WS branching fraction of $R_{WS}^{K\pi\pi^0} = [0.229 \pm 0.015^{+0.013}_{-0.009}]\%$. In 2006 BABAR reported⁵⁰ a measurement of $R_{WS}^{K\pi\pi^0} = [0.214 \pm 0.008 \pm 0.008]\%$. No evidence for CP violation was observed in these studies.

BABAR analyzed the $D^0 \rightarrow K \pi \pi^0$ decay mode using two different methods (see

Table 5. Results for x , y , and y_{CP} from $D^0 \rightarrow K_S^0 \pi^+ \pi^-$ and $D^0 \rightarrow K_S^0 K^+ K^-$ time-dependent analyses. All results are from Dalitz-plot analyses except the Belle y_{CP} result. Uncertainties on x and y are statistical, experimental systematic, and resonance decay model systematic, respectively. From Refs. 46, 47, 48.

Experiment	Fit Type	Parameter	Result	95% C.L. Limit
CLEO ⁴⁷	No CPV	x (%)	$1.8^{+3.4}_{-3.2} \pm 0.4 \pm 0.4$	$(-4.7, 8.6)$
CLEO ⁴⁷	No CPV	y (%)	$-1.4^{+2.5}_{-2.4} \pm 0.8 \pm 0.4$	$(-6.3, 3.7)$
CLEO ⁴⁷	CPV	x (%)	$2.3^{+3.5}_{-3.4} \pm 0.4 \pm 0.4$	$(-4.5, 9.3)$
CLEO ⁴⁷	CPV	y (%)	$-1.5^{+2.5}_{-2.4} \pm 0.8 \pm 0.4$	$(-6.4, 3.6)$
Belle ⁴⁸	No CPV	x (%)	$0.80 \pm 0.29^{+0.09+0.10}_{-0.07-0.14}$	$(0.0, 1.6)$
Belle ⁴⁸	No CPV	y (%)	$0.33 \pm 0.24^{+0.08+0.06}_{-0.12-0.08}$	$(-0.34, 0.96)$
Belle ⁴⁸	CPV	x (%)	$0.81 \pm 0.30^{+0.10+0.09}_{-0.07-0.16}$	$ x < 1.6$
Belle ⁴⁸	CPV	y (%)	$0.37 \pm 0.25^{+0.07+0.07}_{-0.13-0.08}$	$ y < 1.04$
Belle ⁴⁸	CPV	$ q/p $	$0.86^{+0.30+0.06}_{-0.29-0.03} \pm 0.08$	—
Belle ⁴⁸	CPV	$\arg(q/p)$ ($^\circ$)	$14^{+16+5+2}_{-18-3-4}$	—
Belle ⁷⁴	No CPV	y_{CP} (%)	$0.11 \pm 0.61 \pm 0.52$	—
BABAR ⁴⁶	No CPV	x (%)	$0.16 \pm 0.23 \pm 0.12 \pm 0.08$	—
BABAR ⁴⁶	No CPV	y (%)	$0.57 \pm 0.20 \pm 0.13 \pm 0.07$	—
World average ⁷¹	No CPV	x (%)	0.419 ± 0.211	
	No CPV	y (%)	0.456 ± 0.186	

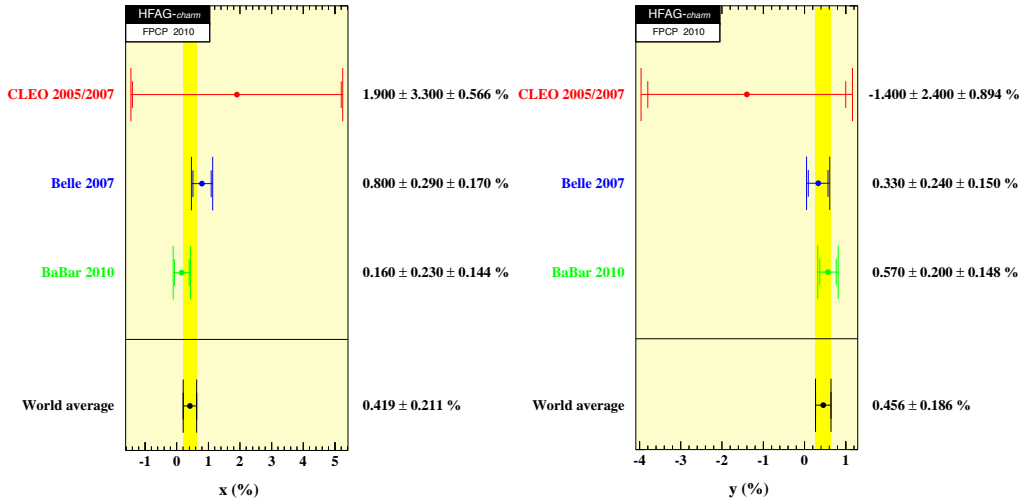


Fig. 25. $K_S^0 h^+ h^-$ world averages for x and y , assuming no CP violation. From Refs. 15, 71.

Sec. 2.3.2). Method I measured the time-integrated mixing rate $R_M = [0.023^{+0.018}_{-0.014} \pm 0.004]\%$ with a 95% CL upper limit of $R_M < 0.054\%$ assuming CP conservation. The result is compatible with the no-mixing hypothesis at the 4.5% CL. Additional

results are given in Table 6. These include measurements allowing for CP violation.

This study estimated systematic uncertainties by varying selection cuts, changing background PDF shapes and the decay-time resolution model, varying the D^0 lifetime, and changing efficiency corrections, and by performing the fit over the full Dalitz-plot phase space. Method I results are statistics-limited.

Table 6. Mixing and CP violation results from $BABAR$ analyses of $D^0 \rightarrow K\pi\pi^0$ using method I and method II (see text for description of parameters).

CP conservation assumed	CP violation allowed
<i>BABAR</i> method I ⁵⁰	
$R_M = (0.023_{-0.014}^{+0.018} \pm 0.004)\%$	$R_M = (0.010_{-0.007}^{+0.022} \pm 0.003)\%$
$\alpha\tilde{y}' = -0.012_{-0.008}^{+0.006} \pm 0.002$	$\alpha\tilde{y}' \cos \tilde{\phi} = -0.012_{-0.007}^{+0.006} \pm 0.002$
	$\beta\tilde{x}' \sin \tilde{\phi} = 0.003_{-0.005}^{+0.002} \pm 0.000$
	$ p/q = 2.2_{-1.0}^{+1.9} \pm 0.1$
<i>BABAR</i> method II ⁵³	
$x'_{K\pi\pi^0} = 0.0261_{-0.0068}^{+0.0057} \pm 0.0039$	$x'^+_{K\pi\pi^0} = 0.0253_{-0.0063}^{+0.0054} \pm 0.0039$
$y'_{K\pi\pi^0} = -0.0006_{-0.0064}^{+0.0055} \pm 0.0034$	$y'^+_{K\pi\pi^0} = -0.0005_{-0.0067}^{+0.0063} \pm 0.0050$
	$x'_{K\pi\pi^0} = 0.0355_{-0.0083}^{+0.0073} \pm 0.0065$
	$y'_{K\pi\pi^0} = -0.0054_{-0.0116}^{+0.0040} \pm 0.0041$
$r_0^2 = (5.25_{-0.31}^{+0.25} \pm 0.12) \times 10^{-3}$	

Method II measured the mixing rate parameters $x'_{K\pi\pi^0}$ and $y'_{K\pi\pi^0}$ assuming CP conservation, and $x'^{\pm}_{K\pi\pi^0}$ and $y'^{\pm}_{K\pi\pi^0}$ allowing for CP violation, where the $+$ ($-$) sign denotes measurement using only D^0 (\bar{D}^0) candidates. The method II results are inconsistent with the no-mixing hypothesis at a significance of 3.2 standard deviations. Mixing parameter values are given in Table 6.

The fit method is validated by generating Monte Carlo datasets using values for the PDF parameters and amplitudes taken from fits to the data. Toy Monte Carlo datasets are generated over the range $[-0.6, 0.6]$ in $[x'_{K\pi\pi^0}/r_0, [y'_{K\pi\pi^0}/r_0]$, and fits to them reconstruct the generated values to within an offset of 30% of the statistical error. Studies show that increased Monte Carlo statistics reduce this offset. The final results include a correction for this effect.

Systematic tests performed in the method II analysis include setting the decay-time resolution mean to zero (fitted value 4.2 ± 0.7 fsec); changing the isobar model by varying the masses and widths of the included resonances within their errors; varying the numbers of signal and background events in each category; and changing the definition of the signal-region and candidate-selection criteria.

3.3.3. $D^0 \rightarrow K^+\pi^-\pi^+\pi^-$ Analysis Results

$BABAR$ has reported a preliminary result⁷⁶ using a time-dependent analysis of the $D^0 \rightarrow K3\pi$ mode to set a limit on the mixing rate of $R_M < 0.048\%$ at the 95%

confidence level ($R_M = [0.019^{+0.016}_{-0.015} \pm 0.002]\%$), and estimates that this is consistent with a no-mixing hypothesis at the 4.5% confidence level. This preliminary result, based on a 230 fb^{-1} data sample, used tagged D^{*+} events to determine the production flavor of the D^0 candidate via the charge of the slow pion π_s and reconstructed the D^0 candidate mass $m_{K\pi\pi\pi}$, the mass difference Δm , the decay time t , and its uncertainty σ_t .

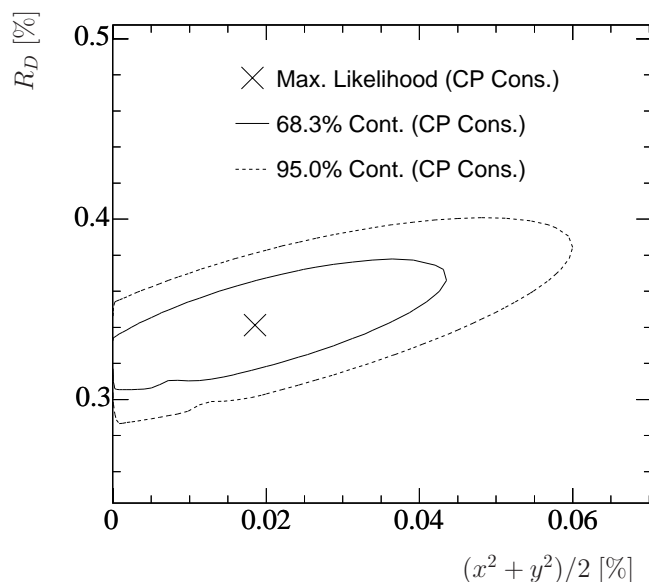


Fig. 26. Likelihood contours from the *BABAR* $K3\pi$ analysis for the CP conserving fit for \tilde{R}_D vs. the mixing rate $R_M = (x^2 + y^2)/2$. Solid line: $\Delta \ln \mathcal{L} = 1.15$; dotted line: $\Delta \ln \mathcal{L} = 3.0$. From Ref. 76.

First, an unbinned extended maximum-likelihood fit is performed simultaneously to the RS and WS two-dimensional distributions $(m_{K\pi\pi\pi}, \Delta m)$. Approximately 3.5×10^5 RS signal candidates are found for D^0 and \bar{D}^0 , respectively, and about 1100 WS signal candidates for each. The much larger RS sample effectively determines the resolution function parameters and D^0 lifetime used in the WS mixing fit. Backgrounds include mis-reconstructed D^{*+} decays, mis-reconstructed charm decays, and combinatorics.

Second, fits to the decay-time distributions are performed. The wrong-sign time-dependence is fitted to

$$\frac{\Gamma_{\text{WS}}(t)}{\Gamma_{\text{RS}}(t)} = \tilde{R}_D + \alpha \tilde{y}' \sqrt{\tilde{R}_D} (\Gamma t) + \frac{(x^2 + y^2)}{4} (\Gamma t^2), \quad (71)$$

where a tilde accent indicates quantities that are integrated over a region of phase

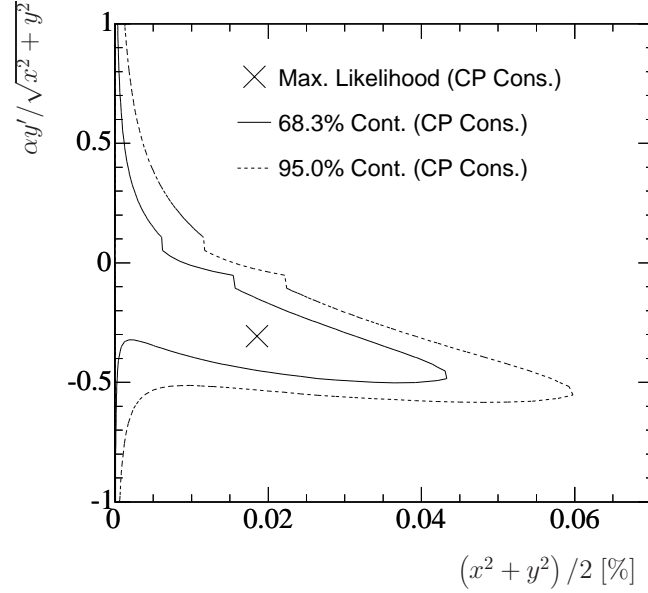


Fig. 27. Likelihood contours from the *BABAR* $K3\pi$ analysis for the CP conserving fit for the interference term vs. the mixing rate $R_M = (x^2 + y^2)/2$. Solid line: $\Delta \ln \mathcal{L} = 1.15$; dotted line: $\Delta \ln \mathcal{L} = 3.0$. From Ref. 76.

space. The factor α accounts for strong-phase variation over the region; A CP -conserving fit (which considers D^0 and \bar{D}^0 candidates simultaneously) and a fit that is sensitive to CP violation (which treats them separately) are performed. The substitutions

$$\alpha \tilde{y}' \rightarrow |p/q|^{\pm} (\alpha \tilde{y}' \cos \tilde{\phi} \pm \beta \tilde{x}' \sin \tilde{\phi}), \quad (72)$$

$$x^2 + y^2 \rightarrow |p/q|^{\pm 2} (x^2 + y^2) \quad (73)$$

are made in Eq. 71, choosing the “+” (“−”) sign for D^0 (\bar{D}^0) candidate decays, respectively. The factor β accounts for ϕ variation over the phase space region.

Systematic uncertainties are estimated by varying the selection criteria, the PDF parametrization of the decay-time resolution function, the background PDF shapes, and the measured D^0 lifetime value. The combined systematics are smaller than the statistical errors by a factor of five.

Assuming CP conservation, the *BABAR* preliminary analysis finds $R_M \equiv (x^2 + y^2)/2$ and the effective mixing parameter $\alpha \tilde{y}'$ to be

$$R_M = [0.019^{+0.016}_{-0.015}(\text{stat.}) \pm 0.002(\text{syst.})]\%, \quad (74)$$

$$\alpha \tilde{y}' = -0.006 \pm 0.005(\text{stat.}) \pm 0.001(\text{syst.}), \quad (75)$$

which are consistent with the no-mixing hypothesis at the 4.3% C.L. Allowing for

CP violation, the analysis finds

$$R_M = [0.017^{+0.017}_{-0.016}(\text{stat.}) \pm 0.003(\text{syst.})]\%, \quad (76)$$

$$|p/q| = 1.1^{+4.0}_{-0.6}(\text{stat.}) \pm 0.1(\text{syst.}), \quad (77)$$

$$\alpha\tilde{y}' \cos \tilde{\phi} = -0.006^{+0.008}_{-0.006}(\text{stat.}) \pm 0.006(\text{syst.}), \quad (78)$$

$$\beta\tilde{x}' \cos \tilde{\phi} = 0.002^{+0.005}_{-0.003}(\text{stat.}) \pm 0.006(\text{syst.}). \quad (79)$$

Two-dimensional coverage probabilities of 68.3% and 95.0% ($\Delta \log \mathcal{L} = 1.15, 3.0$, respectively) are shown in Fig. 26 for the doubly Cabibbo-suppressed rate \tilde{R}_D vs. the mixing rate R_M , and in Fig. 27 for the interference term $\alpha y' / \sqrt{x^2 + y^2}$ vs. R_M .

3.3.4. Semileptonic Decays Analysis Results

Results from five analyses using semileptonic D^0 decays are summarized in Table 7. These include results from $\pi^- N$ collisions (E791⁶² at FNAL, 2×10^{10} events) and e^+e^- interactions near the $\Upsilon(4S)$ resonance (CLEO II.V,⁶³ 9.0 fb^{-1} ; Belle,⁶¹ 492 fb^{-1} ; BABAR singly-tagged,⁶⁵ 87 fb^{-1} ; and BABAR doubly-tagged,⁶⁴ 344 fb^{-1}). The world average is shown in Fig. 28. Results from both $K^{(*)}e\nu$ and $K^{(*)}\mu\nu$ decay modes are included.

Table 7. Mixing results using semileptonic D^0 decay modes. Uncertainties are statistical (first) and systematic (second), except as noted.

Experiment	D^0 modes	Results
E791 ⁶²	$Ke\nu$	$R_M = (0.16^{+0.42}_{-0.37})\%$
	$K\mu\nu$	$R_M = (0.06^{+0.44}_{-0.40})\%$
	Combined	$R_M = 0.11^{+0.30}_{-0.27}\%$
		$R_M < 0.50\%$ at 90% CL
CLEO II.V ⁶³	$Ke\nu$	$R_M = (1.10 \pm 0.76)\%$ (stat.+syst. combined)
	$K^*e\nu$	$R_M = (0.0 \pm 0.31)\%$ (stat.+syst. combined)
	Combined	$R_M = (0.16 \pm 0.29)\%$ (stat.+syst. combined)
Belle ⁶¹	$K^{(*)}e\nu$	$R_M = (-0.6 \pm 2.7^{+1.8}_{-2.1}) \times 10^{-4}$
	$K^{(*)}\mu\nu$	$R_M = (5.9 \pm 3.7^{+3.9}_{-4.5}) \times 10^{-4}$
	Combined	$R_M = (1.3 \pm 2.2 \pm 2.0) \times 10^{-4}$
		$R_M < 6.1 \times 10^{-4}$ at 90% CL
BaBar singly tagged ⁶⁵	$K^{(*)}e\nu$	$R_M = 0.0023 \pm 0.0012 \pm 0.0004$
		$R_M < 0.0042$ at 90% CL
BaBar doubly tagged ⁶⁴	$K^{(*)}e\nu$	$R_M = 0.4 \times 10^{-4}$ (central value)
		R_M in $(-2.2, 2.8) \times 10^{-4}$ at 68% CL
		R_M in $(-13, 12) \times 10^{-4}$ at 90% CL

Since the E791 analysis uses identical selections for both RS and WS candidates, systematic uncertainties in the mixing rate measurement largely cancel. Two

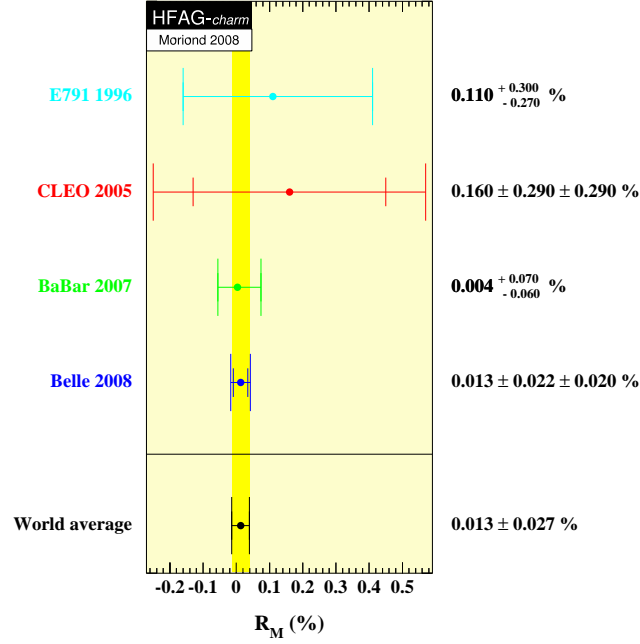


Fig. 28. World average of semileptonic mixing results for R_M in Table 7. Due to possible correlations with the *BABAR* doubly-tagged result, the *BABAR* singly-tagged result is not included in the average. From Ref. 15.

sources of systematic uncertainty that were investigated are the decay-time resolution modeling and feedthrough of hadronic decays into the semileptonic sample. The decay-time determination is subject to detector effects and to the ambiguity from the missing neutrino. Decay times were estimated to be uncertain with a Gaussian smearing of about 15%. This affects the final mixing result by only about 10% of its statistical uncertainty, and is not significant. Feed-through of hadronic events via a hadron mis-identified as a lepton could increase the number of either RS or WS events. The former would overestimate the size of the RS signal and cause an incorrect estimate of the sensitivity to mixing, while the latter would cause a false WS signal. Since RS feed-through was estimated to be very small (about 3%) and, since no WS signal was seen, no corrections were made. Evaluation of the fit modeling systematic uncertainty (performed by adding 10 to 50 simulated mixed events to the WS sample) showed a bias of 10–15% toward a larger mixing rate. Since the final result is an upper limit, no correction was applied.

In the Belle semileptonic result, the main systematics include uncertainty in the signal and background Δm distributions, the amount of RS and WS backgrounds, RS and WS efficiencies, and modeling of the decay-time distribution. These are estimated separately for each of four subsamples, which are categorized by whether the candidate contains an electron or a muon, and which of two silicon vertex

detector configurations was used to record the event. The overall muon sample systematics are about double that of the electron samples, due in part to larger backgrounds in the signal regions.

The CLEO semileptonic analysis uses simulated events to model the background and signal shapes used in the fit. The largest systematic comes from the statistics of the simulation. The second largest systematic is the shape of the decay-time distribution, also obtained from simulation. Other sources of systematic uncertainties are the Q shape (Q = energy released in the D^{*+} decay), electron identification, and fit modeling.

The BABAR singly-tagged semileptonic result systematics include contributions from signal and background PDF shapes, the decay-time resolution model, and decay-time PDFs for background charm decays. Other possible contributions to the systematic on R_M are evaluated and shown to provide no significant contribution. The total systematic error on R_M is about 1/3 of the statistical uncertainty.

The BABAR doubly-tagged semileptonic analysis finds three mixing signal candidates where 2.85 background events are expected. A 50% systematic to the background rate is assigned by comparing ten background control samples with corresponding MC simulations. Other contributions to systematic uncertainties are ignored in comparison to this 50% error. Confidence levels are then calculated for R_M using a frequentist method.

3.4. World Average Results

From HFAG, the world average values for the $D^0\bar{D}^0$ mixing and CPV parameters are shown in Tab. 8. The probability contours, including both statistical and sys-

Table 8. HFAG world average mixing and CPV parameter values.⁷¹

Parameter	No CPV	No direct CPV	CPV -allowed
x (%)	$0.65^{+0.18}_{-0.19}$	0.63 ± 0.19	$0.63^{+0.19}_{-0.20}$
y (%)	0.74 ± 0.12	0.75 ± 0.12	0.75 ± 0.12
$ q/p $	—	1.02 ± 0.04	$0.89^{+0.17}_{-0.15}$
$\varphi(^{\circ})$	—	$-1.05^{+1.89}_{-1.94}$	$-10.1^{+9.4}_{-8.8}$

tematic uncertainties and allowing for CPV , are shown in Fig. 29 for the mixing parameters (x, y) and CPV parameters $(|q/p|, \varphi = \arg(q/p))$. The world average (x, y) excludes the no-mixing point ($x = 0, y = 0$) by 10.1 standard deviations. To date, however, no single measurement exceeds five standard deviations. The no- CPV point ($|q/p| = 0, \varphi = 0$) lies within one standard deviation of the world average ($|q/p|, \varphi$) value. The recent LHCb measurements of mixing and direct CPV ^{28,77} are not included in these averages.

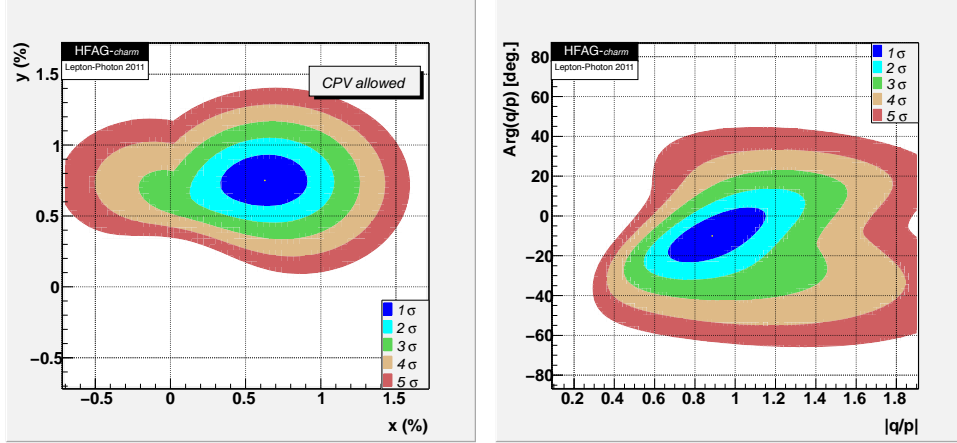


Fig. 29. HFAG world average probability contours⁷¹ for the $D^0\text{-}\bar{D}^0$ mixing parameters (x, y) (left) and for the CPV parameters $(|q/p|, \varphi = \arg(q/p))$ (right).

4. What's Next?

Our understanding of charm physics has made great progress since 1975, when the first evidence for charm mesons was observed. The fact that the no-mixing hypothesis has been excluded by 10 standard deviations, combined with improved understanding of the mechanisms leading to $D^0\text{-}\bar{D}^0$ mixing and CPV , leaves us in a position to make considerable progress in the next few years in the charm sector in both experimental accuracy and theoretical interpretation. Here we survey a few experiments that are likely to further our knowledge of charm physics and mixing over the next few years.

4.1. BES-III

With well over two years of data-taking at the time of this writing, the BES-III experiment at BEPC-II has already surpassed both CLEO-c and BES-II in recorded luminosity.⁷⁸ With over 200 million J/ψ and 100 million ψ' events, the experiment has about $4\times$ the data samples of BES-II and CLEO-c. Performance of the machine is good, with peak luminosities of order $10^{32} \text{ cm}^{-2}\text{sec}^{-1}$.

Of interest in the context of charm mixing is the machine's performance near the $\psi(3770)$, where it has reached a peak luminosity of $5.6 \times 10^{32} \text{ cm}^{-2}\text{sec}^{-1}$ and recorded over 1 fb^{-1} of data in less than a year. BES-III plans to increase the $\psi(3770)$ dataset to 2.5 fb^{-1} in the next year or so, with a goal to eventually reach 10 fb^{-1} . Using the coherent decay techniques discussed earlier, it is clear that BEPC-II and BES-III should be able to substantially improve our knowledge of charm mixing in the very near future.

4.2. *LHCb*

At the time of this writing, LHCb has embarked on its charm physics program using data taken in 2010 and 2011 and has reported results on open charm production^{79,80} and other measurements. Given the detector design which is optimized for heavy-flavor physics, LHCb is expected to provide precision measurements of charm mixing and CP violation parameters in the next few years. First results showing evidence for direct CP violation by measuring the difference between the two time-integrated CP asymmetries $\mathcal{A}(D^0 \rightarrow K^+ K^-)$ and $\mathcal{A}(D^0 \rightarrow \pi^+ \pi^-)$ have already been reported.^{28,81} Results on y_{CP} and A_F are expected soon,⁸⁰ based on analyses of the higher-statistics 2011 and 2012 data samples. Additional competitive charm mixing and CPV measurements are expected to be forthcoming.

4.3. *SuperKEKB and Belle II*

After a decade-long successful program, the Belle detector and the KEKB accelerator stopped operations in June 2010.⁸² Construction of SuperKEKB has started, and work has begun on the Belle II detector. An initial data sample of 5 ab^{-1} is planned to be recorded starting in 2014 with the eventual goal to reach 50 ab^{-1} by 2021–2022.⁸³ With these integrated luminosities, Belle II will have an excellent opportunity to improve on current $D^0\text{--}\bar{D}^0$ mixing and CPV measurements. With 5 ab^{-1} , Belle II is expected to improve the existing statistics-limited measurements of x and y by approximately a factor of two; with 50 ab^{-1} , an additional factor of two.⁸⁴

4.4. *The Super Flavor Factory SuperB*

The recently approved SuperB project⁸⁵ in Italy will be able to contribute substantially to our knowledge of charm mixing and CP violation. Plans call for the SuperB facility to be able to run at the $\psi(3770)$, where a sample of 2×10^9 $D^0\text{--}\bar{D}^0$ pairs is expected to be accumulated. Both avenues are likely to lead to greatly increased understanding of the details of mixing and CPV . Also, like its predecessor *BABAR*, SuperB will be able to make use of the large charm production cross section near the $\Upsilon(4S)$. Estimates of statistical uncertainties using both $K\pi$ and lifetime ratio methods range from $6\times$ to $12\times$ improvements over existing measurements, and possibly even better, depending on how much SuperB's improved decay-time resolution contributes.

5. Summary

Evidence for charm mixing at the level of 1% in the mixing parameters, first reported in 2007 by the *BABAR* and Belle experiments, along with the recent evidence for direct CPV obtained by the LHCb Collaboration, has created renewed interest in the charm sector as a window to new physics. In the near future, BES-III and LHCb

should be reporting new charm results, along with final contributions from *BABAR*, Belle, CDF, and CLEO. In the next several years, SuperKEKB and SuperB should improve the precision of mixing and CPV measurements by a factor of ten or more. This will be an exciting time for anyone interested in charm physics or precision flavor physics in general.

Acknowledgments

The authors would like to thank their colleagues for helpful conversations and feedback while preparing this article, including I. Bigi, P. Fisher, K. Flood, J. Hewett, A. Kagan, B. Meadows, M. Peskin, A. Schwartz, M. Sokoloff and W. Sun. The authors also gratefully acknowledge support by the U.S. Department of Energy, and would like to thank CERN and the SLAC National Accelerator Laboratory for their kind hospitality.

References

1. Amitava Datta and Dharmadas Kumbhakar. $D^0\text{-}\bar{D}^0$ Mixing: A Possible Test of Physics Beyond the Standard Model. *Z.Phys.*, C27:515, 1985.
2. Alexey A. Petrov. On dipenguin contribution to $D^0\text{-}\bar{D}^0$ mixing. *Phys.Rev.*, D56:1685–1687, 1997.
3. Eugene Golowich and Alexey A. Petrov. Short distance analysis of $D^0\text{-}\bar{D}^0$ mixing. *Phys.Lett.*, B625:53–62, 2005. 14 pages, 1 figure, 2 tables, revtex Report-no: WSU-HEP-0503.
4. Howard Georgi. $D^0\text{-}\bar{D}^0$ mixing in heavy quark effective field theory. *Phys.Lett.*, B297:353–357, 1992.
5. Thorsten Ohl, Giulia Ricciardi, and Elizabeth H. Simmons. $D^0\text{-}\bar{D}^0$ mixing in heavy quark effective field theory: The Sequel. *Nucl.Phys.*, B403:605–632, 1993.
6. Ikaros I.Y. Bigi and Nikolai G. Uraltsev. $D^0\text{-}\bar{D}^0$ oscillations as a probe of quark hadron duality. *Nucl.Phys.*, B592:92–106, 2001.
7. Adam F. Falk, Yuval Grossman, Zoltan Ligeti, Yosef Nir, and Alexey A. Petrov. The $D^0\text{-}\bar{D}^0$ mass difference from a dispersion relation. *Phys.Rev.*, D69:114021, 2004.
8. Adam F. Falk, Yuval Grossman, Zoltan Ligeti, and Alexey A. Petrov. SU(3) breaking and $D^0\text{-}\bar{D}^0$ mixing. *Phys.Rev.*, D65:054034, 2002.
9. Harry N. Nelson. Compilation of $D^0\text{-}\bar{D}^0$ mixing predictions. 1999. 19th International Symposium on Lepton and Photon Interactions at High Energies, arXiv:hep-ex/9908021.
10. Alexey A Petrov. Charm mixing in the Standard Model and beyond. *Int.J.Mod.Phys.*, A21:5686–5693, 2006.
11. Eugene Golowich, JoAnne Hewett, Sandip Pakvasa, and Alexey A. Petrov. Implications of $D^0\text{-}\bar{D}^0$ Mixing for New Physics. *Phys.Rev.*, D76:095009, 2007.
12. Bernard Aubert et al. Evidence for $D^0\text{-}\bar{D}^0$ Mixing. *Phys.Rev.Lett.*, 98:211802, 2007.
13. M. Staric et al. Evidence for $D^0\text{-}\bar{D}^0$ Mixing. *Phys.Rev.Lett.*, 98:211803, 2007.
14. T. Aaltonen et al. Evidence for $D^0\text{-}\bar{D}^0$ mixing using the CDF II Detector. *Phys.Rev.Lett.*, 100:121802, 2008.
15. D. Asner et al. Averages of b -hadron, c -hadron, and τ -lepton Properties. 2010. arXiv:1010.1589 [hep-ex].
16. John F. Donoghue, Eugene Golowich, Barry R. Holstein, and Josip Trampetic. Dispersive Effects in $D^0\text{-}\bar{D}^0$ Mixing. *Phys.Rev.*, D33:179, 1986.
17. Ikaros I. Bigi and A. I Sanda. *CP Violation*. Cambridge University Press, New York, 2009. ISBN: 978-0-521-84794-0.
18. P. K. Kabir. *The CP Puzzle: Strange Decays of the Neutral Kaon*. Academic Press, Inc., 111 Fifth Avenue, New York, New York 10003, 1968. EAN: 978-0-123-93150-4.
19. K Nakamura et al. Review of particle physics. *J.Phys.G*, G37:075021, 2010.
20. Yosef Nir. *CP violation in and beyond the standard model*. 1999. arXiv:hep-ph/9911321.
21. Yosef Nir. *CP violation in meson decays*. pages 79–145, 2005. arXiv:hep-ph/0510413.
22. Alexander L. Kagan and Michael D. Sokoloff. On Indirect *CP* Violation and Implications for $D^0\text{-}\bar{D}^0$ and $B_s\text{-}\bar{B}_s$ mixing. *Phys.Rev.*, D80:076008, 2009.
23. F. Buccella, Maurizio Lusignoli, G. Miele, A. Pugliese, and Pietro Santorelli. Nonleptonic weak decays of charmed mesons. *Phys.Rev.*, D51:3478–3486, 1995.
24. S. Bianco, F.L. Fabbri, D. Benson, and I. Bigi. A Cicerone for the physics of charm. *Riv.Nuovo Cim.*, 26N7:1–200, 2003. Supersedes hep-ex/0306039.
25. Alexey A. Petrov. Hunting for *CP* violation with untagged charm decays. *Phys.Rev.*, D69:111901, 2004.
26. Makoto Kobayashi and Toshihide Maskawa. *CP Violation in the Renormalizable The-*

- ory of Weak Interaction. *Prog.Theor.Phys.*, 49:652–657, 1973.
27. ed. Harrison, P.F. and ed. Quinn, Helen R. The *BABAR* physics book: Physics at an asymmetric B factory. 1998. SLAC-R-0504.
 28. Matthew Charles. Mixing and CP -violation studies in charm decays at LHCb. 2011. arXiv:1112.4155 [hep-ex].
 29. Joachim Brod, Alexander L. Kagan, and Jure Zupan. On the size of direct CP violation in singly Cabibbo-suppressed D decays. 2011.
 30. Yuval Grossman, Alexander L. Kagan, and Yosef Nir. New physics and CP violation in singly Cabibbo suppressed D decays. *Phys.Rev.*, D75:036008, 2007.
 31. J.L. Rosner et al. Determination of the Strong Phase in $D^0 \rightarrow K^+ \pi^-$ Using Quantum-Correlated Measurements. *Phys.Rev.Lett.*, 100:221801, 2008.
 32. Werner M. Sun. Quantum correlations in charm decays. *Conf.Proc.*, C100901:58–64, September 2010. Physics in Collision (PIC2010).
 33. Maurice Goldhaber and Jonathan L. Rosner. Mixing of Neutral Charmed Mesons and Tests for CP Violation in their Decays. *Phys.Rev.*, D15:1254, 1977.
 34. Michael Gronau, Yuval Grossman, and Jonathan L. Rosner. Measuring $D^0-\bar{D}^0$ mixing and relative strong phases at a charm factory. *Phys.Lett.*, B508:37–43, 2001.
 35. David Mark Asner et al. Determination of the $D^0 \rightarrow K^+ \pi^-$ Relative Strong Phase Using Quantum-Correlated Measurements in $e^+e^- \rightarrow D^0 \bar{D}^0$ at CLEO. *Phys. Rev.*, D78:012001, 2008.
 36. T. E. Coan et al. Absolute Branching Fraction Measurements of Exclusive D^0 Semileptonic Decays. *Phys. Rev. Lett.*, 95:181802, 2005.
 37. Q. He et al. Comparison of $D \rightarrow K_S^0 \pi$ and $D \rightarrow K_L^0 \pi$ Decay Rates. *Phys. Rev. Lett.*, 100:091801, 2008.
 38. Werner M. Sun. Simultaneous least squares treatment of statistical and systematic uncertainties. *Nucl. Instrum. Meth.*, A556:325–330, 2006.
 39. D. M. Asner and W. M. Sun. Time-Independent Measurements of $D^0-\bar{D}^0$ Mixing and Relative Strong Phases Using Quantum Correlations. *Phys. Rev.*, D73:034024, 2006.
 40. D. M. Asner and W. M. Sun. Erratum: Time-Independent Measurements of $D^0-\bar{D}^0$ Mixing and Relative Strong Phases Using Quantum Correlations [Phys. Rev. D 73, 034024 (2006)]. *Phys. Rev.*, D77:019901, 2008.
 41. Tie-hui (Ted) Liu. The $D^0\bar{D}^0$ mixing search: Current status and future prospects. 1994.
 42. E. M. Aitala et al. Measurements of lifetimes and a limit on the lifetime difference in the neutral D meson system. *Phys. Rev. Lett.*, 83:32–36, 1999.
 43. Sven Bergmann, Yuval Grossman, Zoltan Ligeti, Yosef Nir, and Alexey A. Petrov. Lessons from CLEO and FOCUS Measurements of $D^0-\bar{D}^0$ Mixing Parameters. *Phys. Lett.*, B486:418–425, 2000.
 44. Bernard Aubert et al. Measurement of $D^0-\bar{D}^0$ mixing using the ratio of lifetimes for the decays $D^0 \rightarrow K^- \pi^+$, $K^- K^+$, and $\pi^- \pi^+$. *Phys. Rev.*, D78:011105(R), 2008.
 45. Bernard Aubert et al. Measurement of $D^0-\bar{D}^0$ Mixing using the Ratio of Lifetimes for the Decays $D^0 \rightarrow K^- \pi^+$ and $K^+ K^-$. *Phys. Rev.*, D80:071103(R), 2009.
 46. P. del Amo Sanchez et al. Measurement of $D^0-\bar{D}^0$ mixing parameters using $D^0 \rightarrow K_S^0 \pi^+ \pi^-$ and $D^0 \rightarrow K_S^0 K^+ K^-$ decays. *Phys.Rev.Lett.*, 105:081803, 2010.
 47. D.M. Asner et al. Search for $D^0-\bar{D}^0$ mixing in the Dalitz plot analysis of $D^0 \rightarrow K_S^0 \pi^+ \pi^-$. *Phys.Rev.*, D72:012001, 2005.
 48. L.M. Zhang et al. Measurement of $D^0-\bar{D}^0$ mixing in $D^0 \rightarrow K_S^0 \pi^+ \pi^-$ decays. *Phys.Rev.Lett.*, 99:131803, 2007.
 49. X. C. Tian et al. Measurement of the wrong-sign decays $D^0 \rightarrow K^+ \pi^- (\pi^0, \pi^+ \pi^-)$ and search for CP violation. *Phys. Rev. Lett.*, 95:231801, 2005.

52 Chavez, Cowan, and Lockman

50. Bernard Aubert et al. Search for D^0 - \bar{D}^0 Mixing and Branching-Ratio Measurement in the Decay $D^0 \rightarrow K^+\pi^-\pi^0$. *Phys. Rev. Lett.*, 97:221803, 2006.
51. Muriel Pivk and Francois R. Le Diberder. SPlot: A Statistical tool to unfold data distributions. *Nucl.Instrum.Meth.*, A555:356–369, 2005.
52. Paul E. Condon and Paul L. Cowell. Channel Likelihood: An Extension of Maximum Likelihood for Multibody Final States. *Phys.Rev.*, D9:2558, 1974.
53. Bernard Aubert et al. Measurement of D^0 - \bar{D}^0 mixing from a time-dependent amplitude analysis of $D^0 \rightarrow K^+\pi^-\pi^0$ decays. *Phys. Rev. Lett.*, 103:211801, 2009.
54. S. Kopp et al. Dalitz analysis of the decay $D^0 \rightarrow K^-\pi^+\pi^0$. *Phys. Rev.*, D63:092001, 2001.
55. D. Aston, N. Awaji, T. Bienz, F. Bird, J. D’Amore, et al. A Study of $K^-\pi^+$ Scattering in the Reaction $K^-p \rightarrow K^-\pi^+n$ at 11-GeV/c. *Nucl.Phys.*, B296:493, 1988.
56. G. Goldhaber, J. Wiss, G.S. Abrams, M.S. Alam, A. Boyarski, et al. D and D^* Meson Production Near 4-GeV in e^+e^- Annihilation. *Phys.Lett.*, B69:503, 1977.
57. E.M. Aitala et al. A Search for D^0 - \bar{D}^0 mixing and doubly Cabibbo suppressed decays of the D^0 in hadronic final states. *Phys.Rev.*, D57:13–27, 1998.
58. S.A. Dytman et al. Evidence for the decay $D^0 \rightarrow K^+\pi^-\pi^+\pi^-$. *Phys.Rev.*, D64:111101, 2001.
59. J.J. Aubert et al. Observation of Wrong Sign Trimuon Events in 250-GeV Muon - Nucleon Interactions. *Phys.Lett.*, B106:419, 1981.
60. A. Bodek, R. Breedon, R.N. Coleman, William L. Marsh, S. Olsen, et al. Limits on D^0 - \bar{D}^0 Mixing and Bottom Particle Production Cross-Sections from Hadronically Produced Same Sign Dimuon Events. *Phys.Lett.*, B113:82, 1982.
61. U. Bitenc et al. Improved search for D^0 mixing using semileptonic decays at Belle. *Phys. Rev.*, D77:112003, 2008.
62. E. M. Aitala et al. Search for D^0 - \bar{D}^0 mixing in semileptonic decay modes. *Phys. Rev. Lett.*, 77:2384–2387, 1996.
63. C. Cawlfeld et al. Limits on neutral D mixing in semileptonic decays. *Phys. Rev.*, D71:077101, 2005.
64. Bernard Aubert et al. Search for D^0 - \bar{D}^0 mixing using doubly flavor tagged semileptonic decay modes. *Phys. Rev.*, D76:014018, 2007.
65. Bernard Aubert et al. Search for D^0 - \bar{D}^0 mixing using semileptonic decay modes. *Phys. Rev.*, D70:091102, 2004.
66. J.C. Anjos et al. A Study of D^0 - \bar{D}^0 Mixing. *Phys.Rev.Lett.*, 60:1239, 1988.
67. J.M. Link et al. Measurement of the doubly Cabibbo suppressed decay $D^0 \rightarrow K^+\pi^-$ and a search for charm mixing. *Phys.Lett.*, B618:23–33, 2005.
68. R. Godang et al. Search for D^0 - \bar{D}^0 mixing. *Phys.Rev.Lett.*, 84:5038–5042, 2000.
69. Bernard Aubert et al. Search for D^0 - \bar{D}^0 mixing and a measurement of the doubly Cabibbo-suppressed decay rate in $D^0 \rightarrow K\pi$ decays. *Phys.Rev.Lett.*, 91:171801, 2003.
70. L.M. Zhang et al. Improved constraints on D^0 - \bar{D}^0 mixing in $D^0 \rightarrow K^+\pi^-$ decays at BELLE. *Phys.Rev.Lett.*, 96:151801, 2006.
71. Heavy Flavor Averaging Group. Charm physics results. <http://www.slac.stanford.edu/xorg/hfag/charm/index.html>.
72. J. M. Link et al. A measurement of lifetime differences in the neutral D meson system. *Phys. Lett.*, B485:62–70, 2000.
73. S. E. Csorna et al. Lifetime Differences, direct CP Violation and Partial Widths in D^0 Meson Decays to K^+K^- and $\pi^+\pi^-$. *Phys. Rev.*, D65:092001, 2002.
74. A. Zupanc et al. Measurement of y_{CP} in D^0 meson decays to the $K_S^0 K^+ K^-$ final state. *Phys. Rev.*, D80:052006, 2009.
75. G. Brandenburg et al. Rate measurement of $D^0 \rightarrow K^+\pi^-\pi^0$ and constraints on D^0 -

- \bar{D}^0 mixing. *Phys. Rev. Lett.*, 87:071802, 2001.
76. Bernard Aubert et al. Search for $D^0 - \bar{D}^0$ mixing in the decays $D^0 \rightarrow K^+ \pi^- \pi^+ \pi^-$. 2006. arXiv:hep-ex/0607090.
 77. R. Aaij et al. Measurement of mixing and CP violation parameters in two-body charm decays. 2011. arXiv:1112.4698 [hep-ex].
 78. Yangheng Zheng. Current and Future Charm Experiments. 2011. arXiv:1102.4502 [hep-ex].
 79. Marco Gersabeck. Searches for CP Violation in Charm Mixing at LHCb. September 2010. Presented at 6th International Workshop on the CKM Unitarity Triangle, Warwick, UK.
 80. Philip John Hunt. Results and prospects for charm physics at LHCb. *PoS, KRUGER2010:061*, 2011.
 81. R. Aaij et al. Evidence for CP violation in time-integrated $D^0 \rightarrow h^- h^+$ decay rates. 2011. arXiv:1112.0938 [hep-ex].
 82. Henryk Palka. Status of Super-KEKB and Belle II. *Acta Phys.Polon.*, B41:2595–2604, 2010.
 83. T. Aushev. Status and prospects of SuperKEKB collider and Belle II experiment. 2012. arXiv:1201.1248 [hep-ex].
 84. T. Abe et al. Belle II Technical Design Report. 2010. arXiv:1011.0352 [physics.ins-det].
 85. B. O’Leary et al. SuperB Progress Reports – Physics. 2010. arXiv:1008.1541 [hep-ex].